Kaolin occurrence and formation in the Tobeatic shear zone

by
D. M. Forfa

A Thesis submitted to
Saint Mary's University, Halifax Nova Scotia
in Partial Fulfillment of the Requirements for
The Degree of Bachelor of Science in Geology

Saint Mary's University

Approved: Dr. Georgia Pe-Piper
Supervisor
Department of Geology
Saint Mary's University

Dr. Erin Adlakha
Internal Examiner
Department of Geology
Saint Mary's University

Date: December 20, 2022

December 20, 2022

Kaolin occurrence and formation in the Tobeatic Shear zone

by D. M. Forfa

Abstract

Kaolin is found along the south-eastern contact of the South Mountain Batholith and the Meguma metasediments, 21 km along length on strike of the Tobeatic shear zone and on trend with regional folds and faults. The Meguma Terrane, along with the exotic terrane of Avalonia, accreted to ancestral North America (Laurentia) during the Middle Devonian Acadian Orogeny, causing voluminous felsic magmatism. The region remained periodically active throughout the final event of the Appalachian orogen, the Late Carboniferous-Permian Alleghanian orogeny (~310 - 260 Ma). The shear zones are inferred to have been active during the igneous emplacement SMB and remained pathways for late-stage mineralizing fluids during uplift. Kaolin is found associated with several types of mineralization, including base metals (Zn, Sn), Cu and aluminum-phosphate-sulfate minerals (APS). Using optical and SEM petrography, geochemical analysis, including ^{18}O values, the kaolin is characterized, according to morphology, fabric and texture, growth mechanics and formation, as well as mineral and textural associations. Two chemically different types of kaolin are identified. $\delta\,^{18}O$ values provide additional constraints on the sources of the oxidizing fluids, having a significant contribution of meteoric fluids. Relative chronology of formation is inferred, based on types of alteration and temporal events, with quartz and kaolin not forming synchronously along the Tobeatic shear zone.

Acknowledgments

This project would not have been possible without the support of Dr. Georgia Pe-Piper, who as a professor emeritus generously guided me along the thesis process. I am grateful for her knowledge, thoroughness and dedication. I would like to thank Dr. David Piper for his support in sample collection, interpretation of data and feedback during the editing process. I have much to learn from you both.

I would like to thank Dr. Xiang Yang for his assistance in sample analysis on the SEM. I would also like to thank Dr. Jacob Hanley for his assistance with calculations and interpretation of isotope data. To Mick O'Neil for his assistance in locating drill cores at the Stellarton core library. Thank you to my friend and colleague, Fergus Tweedle for his help in collecting samples and offering encouragement.

Finally, thank you to Dr. Erin Adlakha for her valuable comments and questions during the review process. As well as Dr. Mitch Kerr, for assisting with technical details and always being a welcoming presence at the SMU Geology Department.

Thin section preparation was done by Vancouver Petrographics Ltd.
and geochemical analysis (Whole Rock Analysis, Stable Oxygen isotopes) by ActLab.

This project was funded through a Clay Minerals Society student grant.
I am grateful for the analytical opportunities it has afforded throughout this study.

W pamięci, Krystyny Sobocińskiej
1929 - 2012

Głowa do góry

Contents

List of Tables

List of Figures

Abbreviations

Minerals

ab	albite
ap	apatite
chl	chlorite
gcx	gorceixite
kn	kaolin
Kfs	K-feldspar
mag	magnetite
ms	muscovite
pym	pyromorphite
qz	quartz
sme	smectite
Ti-O	Titanium oxide
APS	Alunite-Phosphate-Sulphate minerals

Geology

SMB	South Mountain Batholith
DLP	Davis Lake Pluton
KSZ	East Kemptville shear zone
SRT	Shelburne River Till

Introduction

The focus of this study is a kaolin mineral deposit located along the south-eastern contact of the Davis Lake pluton and the Goldenville Group metagreywacke, along a 21 km strike length of the Tobeatic Shear Zone (MacDonald 2001, Corey and Graves 1996) - sites A - C on map, Figure 1.1 - trending NE 60 degrees. The study area is located in Kespukwitk (Land's End), Mi'kma'ki, the ancestral and unneeded territories of the L'nu; southwestern Nova Scotia, Canada. The geological region is known as the Meguma Terrane, the most easterly terrane of the Northern Appalachians. The Meguma Terrane, along with the exotic terrane of Avalonia, accreted to ancestral North America (Laurentia) during the Middle Devonian Acadian Orogeny, causing voluminous felsic magmatism (Horne et al. 1992). The region remained periodically active throughout the final event of the Appalachian orogen, the Late Carboniferous-Permian Alleghanian orogeny (310 — 260 Ma) (Benn et al. 1999), interpreted as the terminal collision between the two continents, Gondwana and Laurentia, with the final closing of the Rheic ocean leading to the formation of Pangean (Murphy and Keppie 2005).

Kaolin is found along regional NE-SW shear zones, occurring with quartz-breccia or greinsenized granite, between contact of the South Mountain Batholith and the metasedimentary Meguma Terrane, on trend with regional folds. The shear zones are inferred to have been active during the igneous emplacement of the SMB and remained pathways for late-stage mineralizing fluids and silica flooding (Horne et al. 2005, Halter et al. 1998). The geological setting and kaolin mineralogy are detailed in Part A: Literature Review. Source fluids for kaolin formation along the Tobeatic shear zone, has been suggested as a mixture of hypogene and supergene fluids (Kontak and Kyser, 2001). To further constrain kaolin formation, this study characterizes kaolin according

to 1) morphology, 2) fabric and texture, 3) growth mechanics 4) occurrence, as well as 5) mineral associations, through SEM and optical petrography. Relative timing of formation is inferred from kaolin characteristics (e.g. vein cross-cutting, volume reduction), mineral associations, and further constrained by oxygen isotopes analysis of quartz and kaolin samples. All these data are synthesized in a descriptive genetic model in Part B: Theoretical Framework.

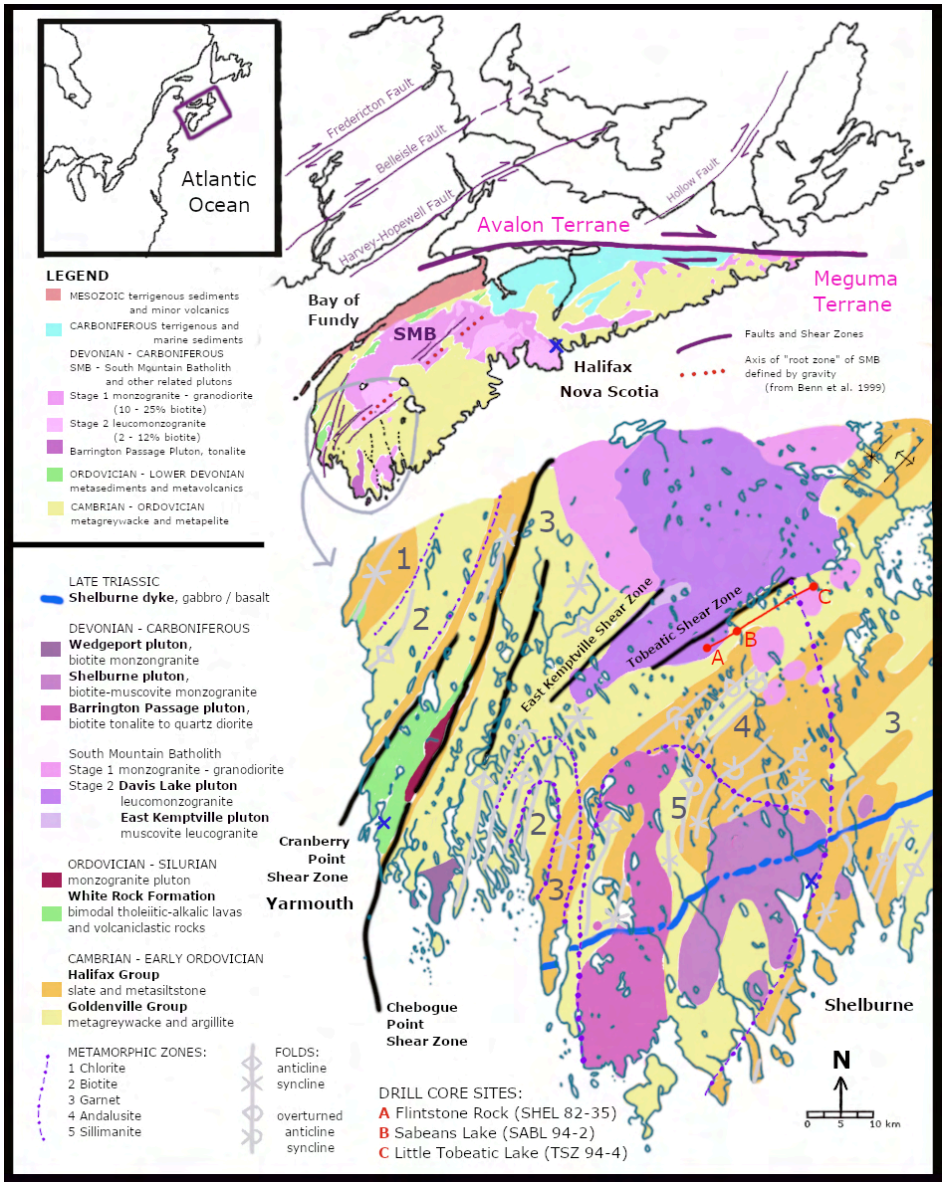

Figure 1.1 Regional geological map of Kespukwitk, Mi'kma'ki; based on sources cited in the text. Three borehole sites marked (A-C), along a 21 km length of the Tobeatic shear zone, in red.

1: Geological Setting of the Tobeatic Shear Zone

1.1 Metasedimentary Meguma Supergroup

The Meguma Supergroup is a thick (>10km) sequence of Cambro-Ordovician flyshoid meta-sedimentary rocks (White 2010). The structural basement of the Meguma terrane is not known but it has been proposed that the terrane was thrust over Avalonia (Shelnutt et al. 2019, Dostal and Chatterjee 2009, Keppie and Krogh 2000). It includes the Cambrian Goldenville Group greenish-grey greywacke and argillite/shales and the Ordovician Halifax Group shale (White 2010, Shelnutt et al. 2019). The unconformably overlying Rockville Notch Group is a sequence of slate, quartzite and bi-modal rift-related volcanic rocks, from the Ordovician to Silurian (ca. 450 Ma to 420 Ma) and with detrital zircon ages that are indistinguishable from the Arisaig Group, suggesting that this group has a greater affinity with the Avalonian terrane (Shelnutt et al. 2019). A nearly concordant U-Pb age of 442 ± 4 Ma has been interpreted as the age of the basal rhyolitic tuff extrusion (Keppie and Krogh 2000). The chemical alkalic affinity of the mafic volcanic rocks and intrusions in the White Rock Formation indicates a continental within-plate setting (MacDonald et al. 2011). SE to NW diachronism is associated with the onset of deformation throughout the Devonian (Murphy and Keppie 2005). The Meguma sediments were variably metamorphosed (greenschist to lower amphibolite facies) and deformed into NE-trending folds during the Early to Middle Devonian (ca. 405-365 Ma) (White 2010). Granulite-facies xenoliths were found within a Late Devonian mafic dyke that also intrudes the Meguma Group (Owen et al. 1988). More significantly, the Meguma sediments were intruded by numerous late syntectonic to post-tectonic peraluminous granitic plutons (MacDonald 2001), overall referred to as the South Mountain Batholith (SMB) - Fig. 1.1.

1.2 Granitoid South Mountain Batholith; Davis Lake Pluton

The Davis Lake pluton (DLP, 800 km^2) forms an elongated southwestern extension to the voluminous but short lived, South Mountain Batholith (SMB, 7300 km^2), ca. 380-370 Ma (U/Pb zircon, Ar/Ar mica) (Dostal et al. 2004). Geochronology and thermochronology suggests emplacement within a narrow time interval of <5Ma (MacDonald et al. 1992, Horne et al. 1992). The South Mountain batholith is a peraluminous granitoid composite intrusion (ie. A/CNK, >1), in which later stage 2 plutons have intruded adjacent to earlier stage 1 plutons (MacDonald et al. 1992). The DLP is one of the stage 2 plutons and consists predominantly of coarse-grained, topaz-muscovite bearing leucomonzogranite (68.5 to 76.3 wt% SiO2) (Dostal et al. 2004, Shellnutt and Dostal 2012). A crystallization age of 378 Ma based on radiometric ages (Rb-Sr, Re-Os, Pb-Pb) has been obtained from the most evolved part of the Davis Lake pluton (Dostal et al. 2004). The DLP is compositionally zoned (margins more felsic) and features N and NE megacryst alignment (Kontak et al. 2001).

The SMB has a sharp intrusive contact with the metasedimentary host rock. A narrow thermal aureole (100 m to 1km) is shown by porphyroblastic growth of andalusite and cordierite, obliteration of slaty cleavage and silification of country rocks (MacDonald 2001). The overall lack of deformation of the country rock, abundance of xenoliths, along with other field evidence has led to the interpretation that the batholith originated by upward movement of magma from partial melting of a deeper protolith (MacDonald 2001). Overall, the average concentrations of major and trace elements suggest a syn- or late-collisional tectonic environment (MacDonald 2001). Unconformably overlying sedimentary rocks of Namurian to Tournaisian (Carboniferous) age in areas of the Meguma terrane, suggest uplift and rapid unroofing of the intrusion within 10Ma (Dostal and Chatterjee 2009).

The mineral potential of the SMB has been under ongoing investigation since the 1970s, with the exploration of the nearby East Kemptville shear zone which borders along the northeastern contact of the Davis Lake pluton. Extensive zones of ore mineralization, including cassiterite, chalcopyrite, pyrite, sphalerite (Sn-Zn-Cu), arsenopyrite (Fe-S), galena (Pb) and gold (Au) have been identified along the East Kemptville shear zone (O'Reilly et al. 2016). Other granite- and metasediment-hosted Sn-Zn-Cu-In mineral occurrences in the region include Duck Pond (Sn), Brazil Lake (Li), Fanning Lake (Au), Pearl Lake (Sn-Cu) and Dominique (Sn) (O'Reilly et al. 2016).

1.3 Hydrothermal Fluid Interactions

Hydrothermal fluids were required to account for the alkali metal enrichment (e.g. Na, K, Rb) in the altered leucogranites of the Davis Lake pluton (Shellnutt and Dostal 2012), but the sources of fluid have not yet been clearly identified. Constraints on fluid chemistry, oxygen fugacity, crystallization temperature and pressure are limited by a succession of overprinting hydrothermal metasomatic events with changes in bulk composition and conditions. Studies of Rb-Sr and $^{40}Ar/^{39}Ar$ ratios in biotite and muscovite from the DLP provide alteration dates ranging from 340 - 250 Ma along the East Kemptville fault zone (Kontak and Cormier 1991); these younger ages are interpreted to reflect the sequence of overprinting tectonothermal events and hydrothermal fluids along the periodically active fault zones. Late Carboniferous magmatism is indicated by a reported U-Pb isotopic age of ca. 316 Ma for the Wedgeport Pluton, exposed along the coast south of Yarmouth (Cormier et al. 2011).

In East Kemptville, the most evolved phase of the DLP, F- and P- rich pegmatites are found within aphanitic felsic dykes, emplaced near the roof zone of the intrusion. Analysis of fluid inclusions hosted in the pegmatitic quartz and cassiterite indicate a highly saline brine of c. 40 wt. % eq. NaCl, its chemistry inferred to be consistent with exsolution from a primary magmatic fluid and modelled isochores constrain formation to c. 550-600 °C (Kontak et al. 2001). Due to the low volume of pegmatite formation, rapid decompression is proposed as the generating mechanism, suggesting emplacement in an existing shear zone environment (Kontak et al. 2001). The separation of fluid from magma is proposed to have occurred at a very late stage, due to a drop in pressure associated with tectonic fracturing prior to final crystallization of the DLP (Halter et al. 1998). The greisen-style mineralization within the East Kemptville shear zone resulted in ore mineralization closer to fracture veins (Halter et al. 1998). The alteration sequence is proposed to have formed in a NaCl magmatic brine with an approximately constant temperature of 450 °C and a pressure of 3.5 ± 1.0 kbars (Halter et al. 1998). The duration of the hydrothermal system associated with greisen formation is estimated to be a maximum of 3 Ma, based on the estimated initial lead isotopic composition and that measured in the mineralized galena; this time frame is considered to be analogous with emplacement of the DLP (Chatterjee and Kontak 1992). Whole-rock fractionation of stable oxygen isotopes indicate that other fluids infiltrated and some mixing did occur along the contact (Kontak et al. 1991, Kontak et al. 2001). The low Fe/(Fe+Mg) ratio of biotites in the East Kemptville imply hydrothermal fluid with higher oxygen fugacity, which could be caused by presence of meteoric fluids or other process (e.g. release of H_2 gas or formation of H_2S) (Corey 1988). The infiltration of supergene fluids along the regional faults may be associated with extensive hematite alteration, U (e.g. Millet Lake) and Mn (e.g. New Ross area) deposits (Kontak and Kyser 2000).

Gravity data of the SMB indicate a long NE-SW root extending from the East Kemptville area, through the southern margin of the East Dalhousie pluton to north of the New Ross pluton, corresponding with the regional fault zone. This is reflected in the shear zones parallel orientation to a regional structural grain in the Meguma group and has been interpreted as a feeder channel for magma (Benn et al., 1999), reflecting the flow pattern of upwelling magma during emplacement. A hypogene source of fluids has been suggested for the New Ross Mn deposit (O'Reilly 1992), located in the New Ross pluton of the SMB, on trend with the regional structurally controlled NE-SW deformation zones. Brecciation and hydrothermal alteration along these zones persist to at least 452 m below the New Ross mine workings (O'Reilly 1992). The large slab-like body of the SMB is deepest within the New Ross pluton, its main stalk reaching a depth of 20 to 25 km (Douma 1978).

1.4 Structural Geology and Tectonic Evolution

The accretion of the Avalonia and Meguma terranes was part of a series of tectonic events, accompanying the amalgamation of composite terranes leading to the closure of the Iapetus and Rheic oceans (Murphy and Keppie 2005, Keppie et al. 2021). Despite several decades research determining the complex sequence of tectonic events and underlying mechanisms, uncertainties remain. A NE-SW Appalachian fault trend has been observed inland along faults of the previously accreted terranes (e.g. Belleisle fault) and can also be found in Nova Scotia (e.g. Hollow Fault) (Waldron et al 2015). The orientation of the Meguma Terrane does not fit the fault trend of the Canadian Appalachians, as the Meguma Terrane docked along a major E-W fault zone and this oblique collision resulted in dextral transpression and induced rapid vertical uplift (Murphy and Keppie 2005) during the Devonian that continued throughout the late

Paleozoic age (Fig. 1.2). The Acadian orogeny has several characteristics: the voluminous felsic magmatism of the SMB, accompanying regional high-T, low-P metamorphism, magmatic fluid circulation emplacing gold deposits and associated siderophile elements, and the rapid Late Devonian exhumation attributed to dynamic uplift (Murphy and Keppie 2005). An interpretation for the mechanism of the tectonic activity is a plume-trench collision, with plume-derived melting causing a flattening of the subduction zone as a result of a collision with the oceanic plateau. It has been proposed that the Acadian orogeny is consistent with flat-slab subduction (Murphy and Keppie 2005) and that the entire South Mountain Batholith has been emplaced along a crustal scale structure (Horne et al. 1992, Shellnutt and Dostal 2012). While the SMB intrusions generally intersect the regional fold pattern of the host Meguma Group without disruption, some features contradict a strictly post-tectonic emplacement, and a syn- or late-collisional tectonic environment has been generally accepted (MacDonald 2001, Shellnutt and Dostal 2012).

A protractacted history of dextral strike-slip deformation is manifested along the major anastomosing Cobequid-Chedabucto fault zone (Mawer and White 1987), between the Meguma and Avalonia terranes. Numerous NE-SW and E-W deformation zones, regional localized and fault zones and shear zones, have been mapped throughout southwestern Nova Scotia (Ham and MacDonald 1991, MacDonald et al. 1992) and can be associated with emplacement of the intrusions (Horne et al. 1988, Horne et al. 1992, Horne et al. 2005). The extent of the movement which occurred along the Cobequid-Chedabucto fault system has been difficult to estimate, between two to three hundred kilometers has been proposed (Waldron et al 2015).

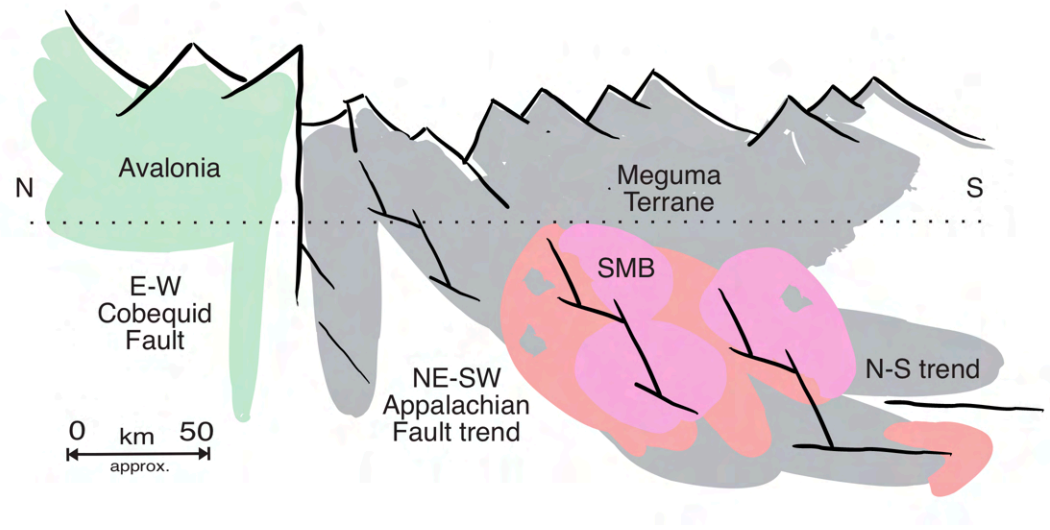

Figure 1.2 Illustration of spatial and temporal relationships observed and inferred from bedrock geology and tectonic activity in the region (based on literature cited on pp.7-10). Regional shear zones are on trend with the Appalachian fault trend, active during South Mountain Batholith (SMB) emplacement. N-S trend formed during subsequent dextral transpression and resulting uplift. The horizontal and vertical scales are schematic.

Deformation within the southwestern portion of the SMB has been recognized as shearing along the contacts of granitoid and metasedimentary outcrcops. Several of the brittle-ductile deformation zones are associated with intense silicification and kaolinite precipitation (Kontak and Kyser 2000). Structures in the SMB include NE-trending faults (=045°) and fractures (at 040° and 062°), interpreted as P and R shears (Riedel geometry) with dextral displacement along the faults (Horne et al. 1992). Other structures in the SMB, NW-trending faults and joints, have been interpreted as tension joints and conjugate shear joints (Horne et al. 1992). Repetitive joint and fault formation suggest regional NW-directed transpression until the Permian as uplift accompanied horizontal compression (Horne et al. 2005).

The Davis Lake pluton exhibits prominent southwest elongation which has been determined to coincide with a regionally extensive deformation zone, the East Kemptville - East Dalhousie Fault Zone (Chatterjee and Kontak 1992). The DLP is also aligned with the East Dalhousie pluton. The elongate NE axis of the DLP is partly bound by a series of faults and intense shearing (MacDonald et al. 1992, Horne et al. 2005). It is considered that the regional fault zones were active at the time of emplacement of the Davis Lake pluton and determine the contact boundaries between the granitic pluton and the host metasediments (Horne et al 1992, Kontak and Kyser 2000). The East Kemptville Shear zone (KSZ), which borders the north-western edge of the Davis Lake pluton, defines a distinct, continuous structure with an inferred length of approximately 30 km (Horne et al. 2005). Strike-slip movement was not significant within the shear zone, as indicated by occurrence of sub vertical tectonic contacts within the East Kemptville tin mine (Corey and Graves 1996). Results of a geochronological study of the East Kemptville — East Dalhousie fault zone indicates episodic activity from ca. 366 to 250 Ma (Chatterjee and Kontak 1992, Kontak and Cormier 1991).

A subparallel regional fault zone along the southern boundary of the DLP, referred to as the Rushmere Lake — Tobeatic Lake Fault Zone extends into the surrounding rocks of the Meguma metagreywacke (Chatterjee and Kontak 1992). It exhibits brittle-ductile deformation delineated within both granite and the country rock (Kontak and Kyser 2000). The DLP is most intensely deformed along the southern contact, with brittle features overprinting earlier ductile fabrics (e.g. kink-banded muscovite and stretched K-feldspar megacrysts, and ribbon-textures mylonite with C-S fabrics) observed at several locations along strike within the Tobeatic Fault Zone (Kontak and Kyser 2000, Corey and Graves 1996). The Tobeatic Shear Zone is generally coincident with the SMB contact and comfortable with the N-S magnetic trends on its the

western edge (Corey and Graves 1996). The full strike length of the TSZ is only roughly defined with zones found along strike, from Rushmere Lake to Little Tobeatic Lake, all within the Tobeatic Fault Zone (Kontak and Kyser 2000). Another shear zone further west, the Deerfield Shear Zone, has a distinct N-S trend (Corey and Graves 1996). The structural and metallogenetic significance of the regional shear zones continues to be investigated, with a proposed epithermal-type model (Kontak and Kyser 2000, Corey and Graves 1996). The only identified outcrop of the Tobeatic Shear shear zone is found on Spectacle Lake, along the eastern side of a spit that juts in from the southern side of the lake. It is of a massive milky quartz breccia with angular rock fragments of both the metagreywacke and leucomonzogranite, overgrown by coarse grained comb quartz and further cross-cut by quartz veins (Corey and Graves 1996).

1.5 Surficial Geology

The study area is currently characterized by the gently rolling, boulder-covered granitic semi-barrens. A southeast-sloping terrain ranging in elevation from 160 m in the north to 90 m in the south, all within the Clyde River Watershed, with south-eastward regional drainage flowing overland. The bedrock of the Davis Lake Pluton and adjacent Meguma metasediments is covered by 3 to 20 metres of Pleistocene glacial till, depending on the bedrock topography. The surfical sediments consist of gravely silt and sand, with 1-3% boulders ranging in size from 0.4 to 10 metres in diameter (Hannon and Roy 2005), designated as the Shelburne River Till (SRT). The till includes distinct lithofacies, including an allochthonous granite ablation till that has been transported as much as 11 km south to southeastward, interspersed with a locally derived till unit that is a stony, psammite-dominated, basal melt-out till (Corey and Graves 1996). The SMB sourced clasts have been identified as being about 2-3 km down-ice from the contact zone.

2. Review of kaolin minerals

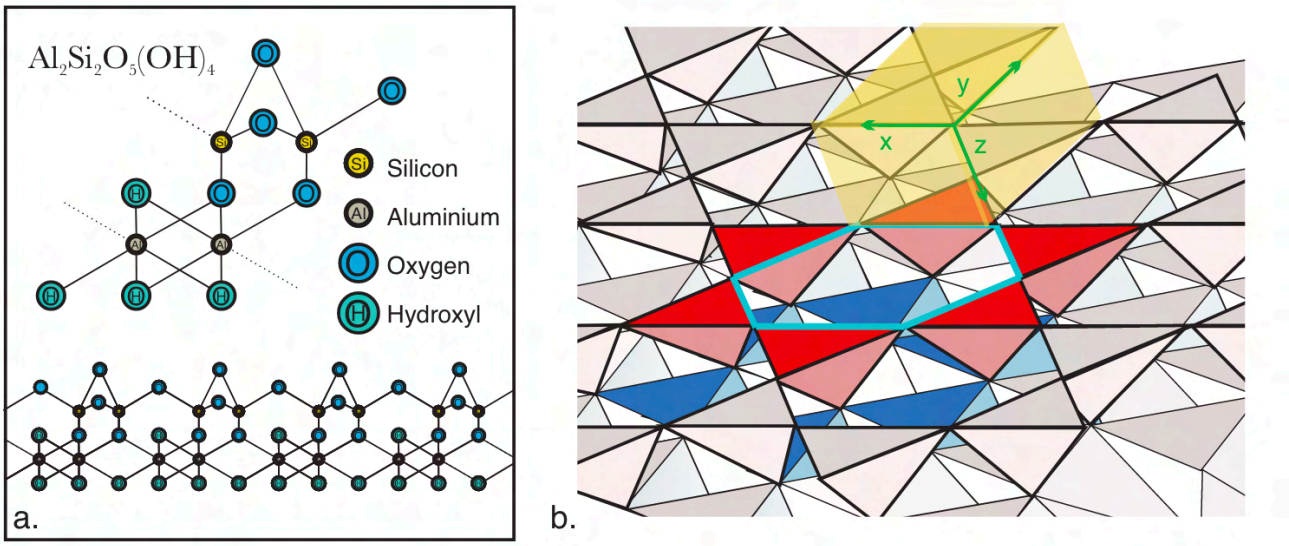

Figure 2.1 Schematic diagrams of the (a) chemical and (b) crystallographic structure of kaolinite. a) Individual kaolinite unit cell and cross-section of T:O lattice, of tetrahedral silica sheet bridged via oxygen to an octahedral gibbsite sheet. b) Three-dimensional view of kaolinite T:O lattice, with isolated six-fold tetrahedral (T) silica ring in red and gibbsite octahedral (O) network in blue. The triclinic crystal structure (in yellow), highlights relative shape and size of unit cell - continuous in the X and Y axes and stacked along the Z axis. Length along the Z axis between two adjacent T:O kaolinite layers is indicated by the basal spacing d=7.16 Å (Poppe et al 2001)

2.1 Mineralogy

Kaolin is a group of phyllosilicate clay minerals. Clay minerals are one of the main rock-forming silicates and are found in abundance in the Earth's crust with oxygen, silicon and aluminium its most important constituents. Clay minerals refer generally to those with a grain size <2 μm (Moore and Reynolds, 1997) and a large ratio of surface area to volume, exhibiting high cation exchange capacity and plastic behaviour when wet. The fundamental unit of all

silicates is the SiO_4 tetrahedron, consisting of four O^{2-} coordinated by one Si^{4+} at the centre. The total binding energy of Si^{4+} is distributed evenly among the oxygen and results in each O^{2-} having potential bonding energy to bridge with another tetrahedral group, in a process referred to as polymerization (Dutrow and Klein, 2007).

The phyllosilicate structure is dominated by a continuous SiO_4 tetrahedra sheet, with three of the four oxygen shared between tetrahedra, resulting in a 2:5 silicon to oxygen ratio (Si_2O_5) (Fig2.1a). A sheet of gibbsite (Al) octahedra coordinate with the silicon tetrahedra sheets, via the apical oxygens (Gardolinski 2005). The six-fold ring of silica tetrahedra surrounds a hydroxyl group (OH) at its centre with the apical oxygens around it. This results in the triclinic structure of kaolinite (Fig.2.1b) where one octahedral sheet interacts with one tetrahedral sheet, referred to as T:O structure or 1:1 layer silicate, with a C1 space group (Dutrow and Klein, 2007). Other structural variations include the geometry of the octahedral sheets, depending on divalent or trivalent cation substitution. Trivalent aluminium is found at the centre of the octahedra, with some Mg or Fe substitution possible, though typically kaolin shows little compositional variety: Al_2O_3 39.6, SiO_2 46.5 and H_2O 14% (Dutrow and Klein, 2007).

The kaolin group includes the dioctahedral member minerals kaolinite, dickite, nacrite and halloysite (Poppe et al., 2001) with kaolinite being the most common (Dutrow and Klein 2007, Gardolinski 2005). It is not possible to properly distinguish kaolin clay minerals of similar composition without X-ray diffraction techniques (Poppe et al., 2001). The use of the terms 'kaolin' and 'kaolinite' coincides with the AIPEA recommendations (Guggenheim et al. 1996), where 'kaolin' is used to identify the entire group and 'kaolinite' refers to the specific polytype, as compared to dickite, nacrite or halloysite.

2.2 Origin of Kaolin

Kaolin is found in both sedimentary (secondary) and igneous (primary) settings, formed through low-temperature, low-pressure reactions with an aqueous fluid; a product of the decomposition of common rocks. In this study, the focus is on the interaction between felsic igneous rock and an acidic, oxidizing fluid present during late stage mineralization. Examples range from the rhyolitic tuffs of Jiangxi, China and the Simav Graben, Turkey (Yuan et al. 2014, Ece et al. 2009); to deposits derived from the coarse-grained granite of Devon and Cornwall, UK and the Bohemian Massif, Czech Republic / Austria (Dominy and Camm 1998, Hohn et al. 2014). The circum-Pacific Rim fold belt hosts many kaolin deposits of both hypogene or supergene origin, sometimes located in close vicinity of each other (Dill 2003). Kaolin formation is understood to be controlled by aluminum silicate dissolution, particularly feldspar, and the accompanying precipitation of oversaturated quartz (Psyrillos et al. 1998). Pseudomorphs after potassium feldspar occur in Cornwall, England (Dutrow and Klein 2007).

The initial fluid composition and the pH of the fluids must lie within the kaolinite stability field, with 300°C as the upper limit. The K+ concentration and pH are two competing factors of the equilibrium constant, with the mineral stability in fluid composition expressed as activity of $SiO_2(aq)$ with K^+/H^+ (Fig. 2.2). The formation of kaolin following the dissolution of feldspar can be expressed as the following chemical hydrolysis reactions, following a fluid evolution path:

$$2KAlSi_3O_{8\ \text{K-feldspar}} + 2H^+ + 9H_2O \rightarrow Al_2Si_2O_5(OH)_{4\ \text{kaolinite}} + 4HSiO_{4\ (aq)} + 2K^+$$

$$2NaAlSi_3O_{8\ \text{Na-plagioclase}} + 2H^+ + 9H_2O \rightarrow Al_2Si_2O_5(OH)_{4\ \text{kaolinite}} + 4HSiO_{4\ (aq)} + 2Na^+$$

These reactions include a release of silica, which is expected to precipitate as quartz, chalcedony, or opal, either inside of pores created by feldspar dissolution or as quartz overgrowths around igneous quartz crystals (Psyrillos et al. 1998). K-feldspar and albitic feldspar (An_{0-20}) typically alter to kaolin via an intermediate mineralizing state of mica (illite) + smectite. Kaolinization of micas can occur from mechanical modification of mica crystals along cleavage planes by precipitating kaolin or replacement (Bristow and Exley 1994, Psyrillos et al. 1998). Plagioclase shows greater sensitivity to alteration and dissolution compared with K-feldspar. The coexistence of kaolinite and smectite is not an equilibrium assemblage: geochemical modelling indicates that upon complete dissolution of feldspars in the rock and an excess in fluid SiO_2 activities, smectite reacts to form kaolin (Psyrillos et al. 1998). Dense arrays of fluid conduits, such as stockworks of quartz veins are susceptible to such alteration leading to an absence of smectite, with the hydrolysis reactions favouring kaolin genesis (Fulgignati 2020).

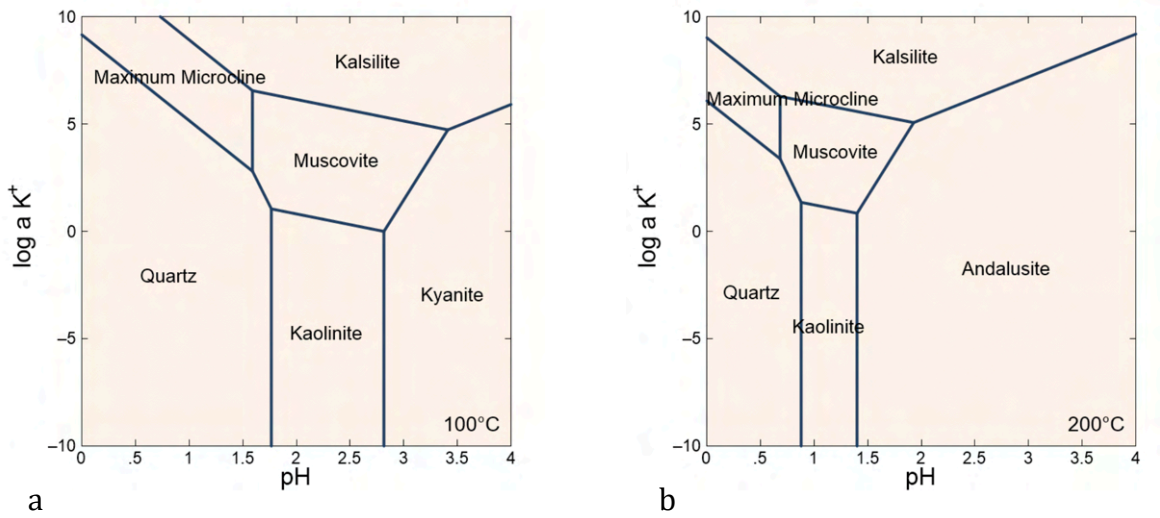

Figure 2.2 - Geochemical stability diagram, showing Si_2(aq) in relation to log aK^+ / pH, at temperatures of (a) 100 °C and (b) 200 °C with P=3bars; no variation in stability at P range of 2-4 bars. SiO_2(aq) activity = 10^{-1}, $a(Al^{+3})=10^{-1}$, $a[O_2(aq)]=10^{-3}$, and $a(H_20)=1$ as main solvent. Modelled using GeoChem Workbench, Act2 (Parkhurst 1995, Bethke et al. 2022)

Kaolin is a key mineral in the intermediate argillic hydrothermal alteration facies occurring at low fluid temperatures (T < 150 - 200°C) through hydrolysis reactions (H+) (Fulgignati 2020). A contraction of the granites occurs in response the kaolinization, due to volume loss, with an estimated 27% of chemical components being leached (Bristow and Exley 1994). Multiple growth stages and a variety of classic epithermal textures, including comb, plumose, and banded, are indicative of the low confining pressures. Interrelationship of aluminum-phosphate-sulphate (APS) minerals with kaolin has been determined to be useful for characterizing physicochemical (i.e. temperature) redox conditions of formation, providing some constraint on temperature during alteration. Such APS minerals (alunite-supergroup) are indicative of a hydrothermal or magmatic origin (Fulgignati 2020).

2.3 Descriptive genetic models

A genetic model for kaolin mineralization in the study area, along the northeast-southwestern strike of the Tobeatic Shear Zone, has not yet been established. The quartz-kaolinite is associated with intense deformation along a considerable strike length; deformed areas of granite are intensely silicified and/or replaced with kaolin within the mineralized structure, as fracture filling, breccia matrix and as a primary clay produced by intense kaolinization of the host rock (Kontak and Kyser 2000, Corey and Graves 1996). The source of the mineralizing and/or altering fluid has not yet been identified and the proximal relationship between kaolin and quartz not been determined.

Fluid inclusion isochores for quartz from Flintstone Rock indicate a maximum P of ca. 1.2 - 2.7 bar at 300°C, the upper limit of kaolinite stability, while the maximum pressure during formation of the South Mountain Batholith (SMB), as indicated by the contact aureole, is 3.2 to 3.5 kbar (Kontak and Kyser 2000). The pressure differential has been interpreted to indicate a confining pressure somewhere between lithostatic and hydrostatic, with an open and connected network of fractures allowing for the infiltration of low-salinity fluids at a depth of ca. 10 km and temperatures of about 250 °C at a typical continental geothermal of 25 °C per km (Kontak and Kyser 2000).

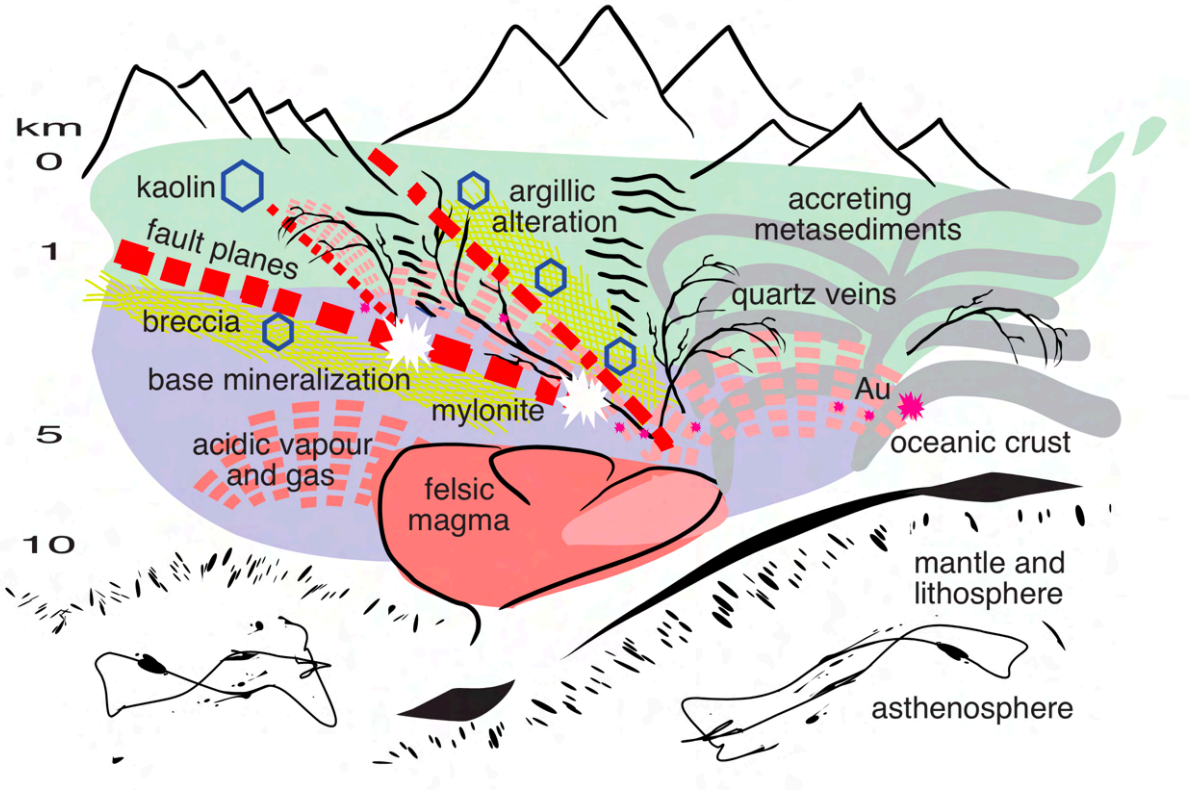

Figure. 2.3 Model of epithermal origin for kaolin in a syn-orogenic setting. Spatial and temporal relationships not to scale. Argillic alteration includes APS minerals. Host rock coloured purple to represent area affected by hydrothermal fluids and blue-green for meteoric water. Illustration based on current literature and knowledge.

Fluid inclusions in quartz sampled at Flintstone Rock, have recorded a low salinity fluid with Na, K, and Ba in solution, consistent with the extensive dissolution of feldspar throughout the DLP (Kontak and Kyser 2000). A continuum is observed from high temperatures and saline fluids of East Kemptville - through 400°C / ca. 20-25 wt% eq. NaCl at Little Tobeatic Lake, to ca. 200 °C / 0 wt. % eq. NaCl at Flintstone Rock (Corey and Graves 1996). Quartz from drill core TSZ94-4 has been found to include three distinct populations of fluid inclusions (Kontak and Kyser 2000):

a. low temperature (100-200 °C), low salinity (<5 wt. % NaCl);

b. moderate temperature (150 - 250 °C), moderate salinity (12 - 18 wt. % NaCl)

c. high temperature (> 300 °C), high salinity (> 20 wt. % NaCl)

Previously sampled sections at 7 m and 129 m in drill hole TSZ94-4 revealed hydrocarbons indicating a magmatic origin. The fluid is inferred to have cooled very quickly to below the upper boundary of the oil window at approximately 150 °C, as there was no degradation of the bitumen (Corey and Graves 1996). The presence of barite, adularia and Zn-Fe-Pb-Cu sulphides at Little Tobeatic Lake has also been noted as a signature of magmatic fluids (Corey and Graves 1996). For comparison, the geochemical modelling of aqueous fluids associated with the primary kaolin deposit of Cornish Clay in England and France, most extensively within the Cornubian batholith (Late Carboniferous to Early Permian), has focused on supergene sources; including meteoric water (pH≈5) and fluids of low salinities (pH≈4) associated with clastic aquifers, at equilibrium conditions and temperatures ranging from 25 - 100 °C (Psyrillos et al. 1998). This estimate is based on the assumption that quartz does not precipitate at temperatures less than 100 °C due to kinetic constraints and a total reaction time of 10 000 years is needed to complete feldspar dissolution (Psyrillos et al. 1998).

Two published $\delta^{18}O$ values for kaolinite samples from Flintstone Rock are consistent at ca. 14‰ but not in isotopic equilibrium with the associated quartz, for deposition at 200-300°C (Kontak and Kyser 2000). The previous stable isotope data for quartz from Flintstone Rock record contrasting values for oxygen ($\delta^{18}O$ = 9.8, 10.4, 15.5 ‰) (Kontak and Kyser 2000), which has been interpreted to indicate a two-fluid mixing model, of both magmatic and meteoric origin. Mineralogically distinct generations of kaolinite may be present within the repeatedly brecciated fault zone at Flintstone Rock (Kontak and Kyser 2000). The interpretation of the genesis of kaolin thus remains uncertain, with possibilities including a supergene formation through weathering of an unroofed pluton under sub-tropical conditions; or a hydrothermal origin associated with late magmatic fluids, as an extension of the Sn-base metal mineralization and greisenization. The alteration and mineralization documented within the study area, up to now, has mineralogical and textural similarities with epithermal-type deposits (Fig. 2.3).

2.4 Kaolin Textures

Stockworks of braided quartz-breccia, providing multiple pathways for fluid migration, have been previously observed with several types of siliceous breccia textures distinguished. Corey and Graves (1996) invoked fluid flow along pre-existing veins and fractures. They inferred that pathways were created by the shearing, stretching the rigid quartz into a series of massive boudins, with the more ductile, plastic kaolinite filling in around the brecciated quartz (Corey and Graves, 1996). Kaolin is commonly found filling vugs within the polyphase quartz veins and along fractures in the abundant and massive, matrix-supported, milky quartz-breccia (Corey and Graves, 1996).

3. Methodology

3.1 Sample Selection

Mineral License Reports (MacGillivray and Shaw 2001a, 2001b, 2001c) and the Resource Report (Hannon and Roy 2005) were reviewed. Initially, a drillcore from the FR (Flintstone Rock) series were not available (Fig. 3.1). Martin MacKinnon, then financial director of Black Bull Resources was contacted, as the drillcores were privately stored in a warehouse in Southwest Nova Scotia but their whereabouts are unknown. A drillcore from the initial 1982 SHEL exploration series was selected instead, as these are stored at the core library in Stellarton. SHEL 82-35 was the only one to intersect quartz breccia along its full length and contained substantial kaolin. It was logged (Appendix 1A) and rock samples were collected on February 18 2019, Table 1.1. Two additional boreholes were selected along the Tobeatic shear zone, drilled as part of a Department of Natural Resources exploration initiative (Corey and Graves 1996). Rock samples from drillcores, TSZ-94-4 and SABL-94-2 were sampled on October 5 2020 at the core library in Stellarton, Appendix 1B and 1C; Table 1.1. Seventeen polished thin sections (30 microns, 26x46mm glass slide) were completed by Vancouver Petrographics Ltd, Table 1.1.

3.2 Optical Microscope

A BX53M Olympus polarizing microscope was used as a verification tool for mineral grain identification to supplement EDS analysis, and provide clarification on crystal structure and textural relationships. Optical properties of grains were observed in plane polarized and cross polarized light.

			Core length		Actual depth				
Drill Core	**Sample #**	REF.	**(m)**	**(ft)**	**(m)**	**PLS**	**SEM / EDS**	**Isotope 18O**	**WRA Analysis**
Little Tobeatic Lake TSZ94-4	27-1		173	567.5	132.52	---	---	---	---
	27-2	C1	165.4	542.5	126.70	TSZ27-2	Oct 25 2021	---	---
	25-1	C2	161.5	530	123.71	TSZ25-1	Oct 25 2021	---	---
	24-1		154.3	506.5	118.19	---	---	---	---
	23-1	C3	150.4	493.5	115.21	TSZ23-1	---	---	---
	22-1		142.8	468.5	109.38	---	---	---	---
	17-1	C4	114	374	87.32	TSZ17-1	Oct 25 2021	---	---
	17-2		114.6	376	87.78	---	---	kao	TSZ4-17-2
	16-1		104.8	344	80.28	---	---	---	---
	16-2	C5	103.6	340	79.36	TSZ16-2	Oct 25 2021	---	---
	15-1	C6	98.2	322	75.22	TSZ15-1	Oct 25 2021	---	---
	14-1		91	298.5	69.71	---	---	---	---
	11-1		69.2	227	53.01	---	---	---	---
	10-1		61.3	201	46.96	---	---	---	---
Sabeans Lake SABL 94-2	21-1		155.4	510	119.04	---	---	---	---
	16-1	B2	100	367	76.60	SAB16-1	Feb 1 2021	---	---
	13-1		95	312	72.77	---	---	---	---
	11-1	B1	80	262.5	61.28	SAB11-1	March 9 2021	---	---
	10-1	^	76.8	252	58.83	---	---	kn	---
	5-1		41.6	136.5	31.87	---	---	---	---
Flintstone Rock SHEL082-35	35-17a *	A5			same	35-17a	---	---	---
	35-17b *		17	55.5		35-17b	Feb 1 2021	---	---
	35-33	A4	33	108		35-33	---	---	---
	35-53a	A3	53	174		35-53a	Dec 21 2020	qz	---
	35-53b		53	174		35-53b	Dec 21 2020		---
	35-60a	A2	60	197		35-60a	---	qz	---
	35-60b		60	197		35-60b	Dec 14 2020		---
	35-66a *	A1				35-66a	Dec 21 2020	qz / kn	---
	35-66b *		66	216.5		35-66b	Dec 14 2020		---

Table 1.1. Summary of collected samples from drillcores SHEL83-35, SABL-94-2 and TSZ94-4 and conducted analysis: polished thin section (PLS), SEM/EDS, Isotope 18O and Whole-Rock Analysis (WRA).

3.3 Scanning Electron Microscope (SEM) / Energy Dispersive Spectroscopy (EDS)

Thirteen of the seventeen polished thin sections were analyzed using the TESCAN MIRA 3LMU Variable Pressure Schottky Field Emission Scanning Electron Microscope at the Regional Analysis Center at Saint Mary's University. The SEM has a maximum resolution of 1.2 nm at 30kV. It is equipped with an Oxford INCA X-Max 80mm^2 silicon drift detector (SDD), which was used to obtain Energy Dispersive Spectroscopy (EDS) chemical analysis. Images were captured using back-scattered (BSE) and secondary (SE) electron imaging. Selected grains were analyzed with an acquisition time of 30 - 45 seconds with an electron beam size of about 10 microns and a working distance of about 17mm.

3.4 Mineral Identification

Mineral identification was determined using the chemical analysis obtained through the EDS, supplemented with BSE images. Brightness and characteristics of the grain were used for identification purposes. Indistinguishable grains have been left out of geochemical analysis.

3.5 Major and trace elements determinations

One whole-rock sample from TSZ 94-4 was analyzed using inductively-coupled plasma optical emission and mass spectrometry (ICP-OES/ICP-MS). Five grams of rock sample, including quartz fragments and powdered kaolin were weighed and send to ActLabs for analysis. Lithium metaborate and lithium tertaborate were used as a flux. Fusion was completed in an induction furnace. The melt was dissolved in a solution of 5% nitric acid. The sample was analyzed for major and trace elements (Ba, Be, Sc, Sr, V, Y, and Zr). The sample was further analyzed using ICP-OES/ICP-MS with sodium peroxide fusion for full suite of trace elements. Values for base metals Cu, Pb, Zn, Ni and Ag, as well as As, Sb, high W > 100ppm, Cr > 1000ppm and Sn >50ppm provided by Fusion ICP/MS are order of magnitude only.

3.6 Oxygen Isotopes (ISO)

Samples of quartz and kaolin were prepared by separating the mineral from the rock sample, fragments of quartz and powdered kaolin (0.5 gram each). The kaolin was sieved using #80 mesh (177 microns). It was determined for three quartz samples from borehole SHEL 82-35 and three kaolin samples (one from each borehole, SHEL 82-35, SABL-94-2 and TSZ 94-4) at ActLabs. Samples were reacted with BrF_5 at ~650 °C in nickel bombs following the procedures described in Clayton and Mayeda (1963). The fluorination reaction converts O in the mineral(s)

to O_2 gas, which is subsequently converted to CO_2 gas using a hot C rod. All reaction steps are quantitative. Isotopic analyses are performed on a Finnigan MAT Delta, dual inlet, isotope ratio mass spectrometer. The data are reported in the standard delta notation as per mil deviations from V–SMOW [$\delta^{18}O = (^{18}O/^{16}O$ sample / $^{18}O/^{16}O$V–SMOW – 1)]. External reproducibility is ± 0.19‰ (1σ) based on repeat analyses of internal white crystal standard (WCS), with a value for NBS 28 of 9.61 ±0.10‰ (1σ). Isotopic fractionation (1000ln α) between quartz, kaolin and fluid (H_2O) was obtained from databases (Vho et al. 2020, Méheut et al. 2007) Fluid-rock reactions with H_2O were complete with online calculators and the Global Seawater Oxygen-18 Database (Schmidt et al. 1999) were used to constrain and correlate isotopic values for H_2O.

3.7 Software Used

All figures and appendices were created using CorelDRAW. Extensions written by Dr. Xiang Yang at Saint Mary's University Regional Analytical Centre were used to format the SEM appendixes. Petrographic photomicrographs were obtained using the software Stream Basic. Stability diagrams were completed in Geochemist's Workbench using Act 2. Oxygen isotope fractionation calculations completed using Alpha Delta, an online tool hosted by Universite Laval, Quebec. Other online tools used during this study are the Peleolatitude Calculator for Paleoclimate Studies (paleolatitude.org) and the Online Isotopes in Precipitation Calculator (OIPC) (waterisotopes.org).

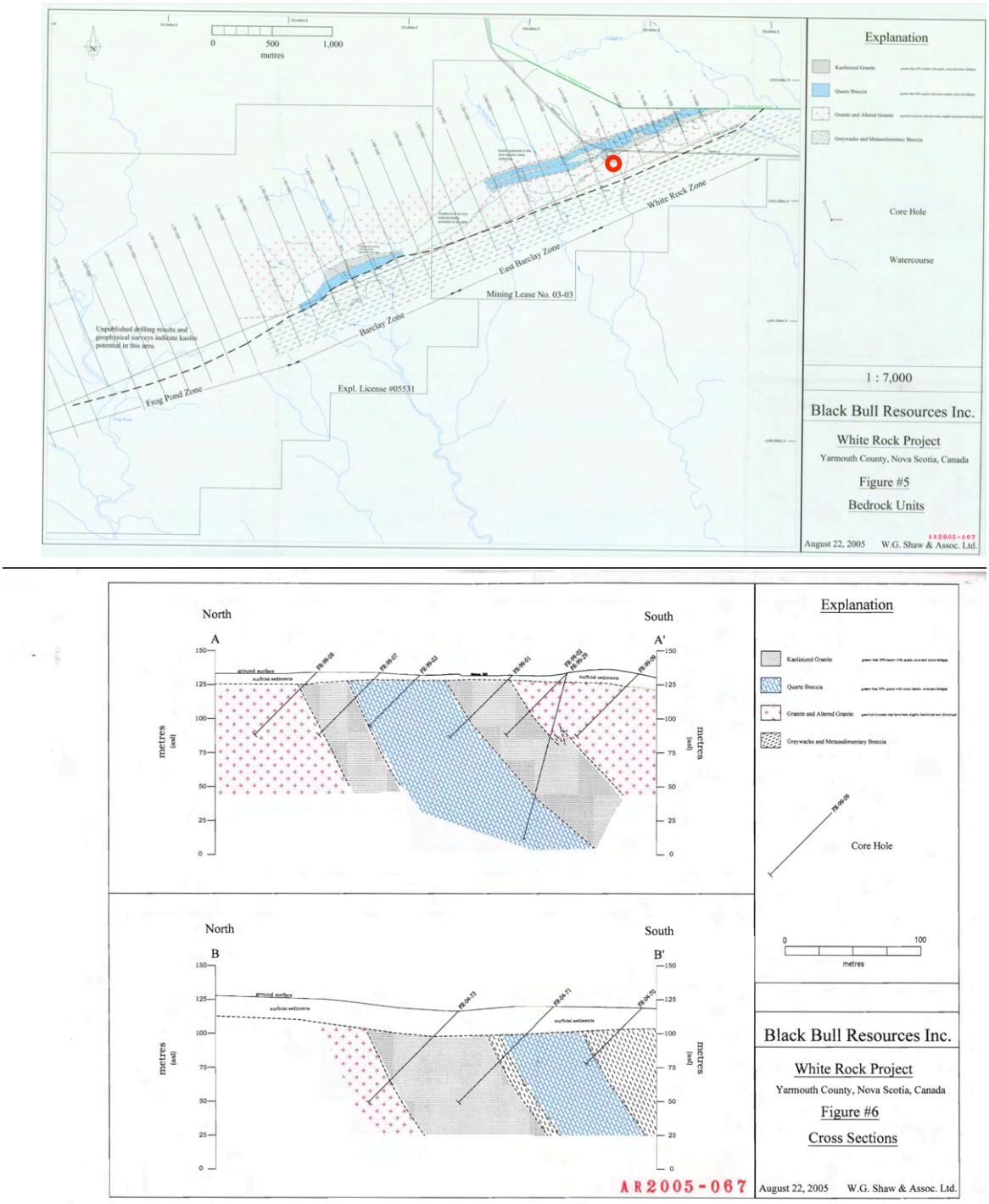

Figure 3.1 Mineral resource maps of Flintstone Rock constructed by Shaw (2005) for Black Bull Resources; showing bedrock units (above) with approximate location of SHEL 82-35 marked with red circle. A - A' cross-section (below) is located in vicinity of the borehole.

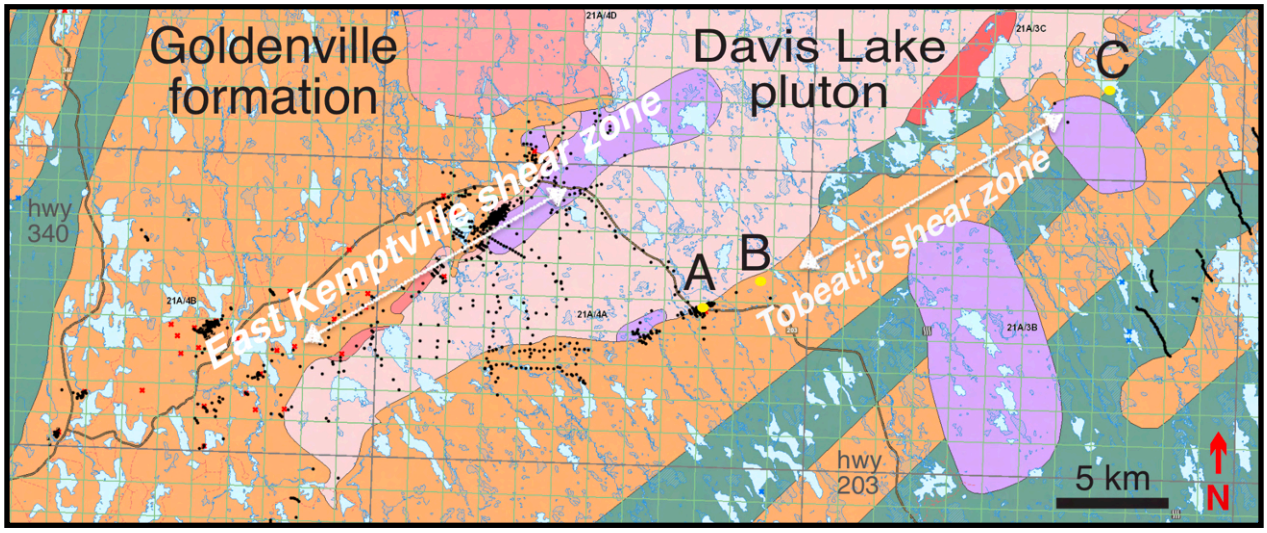

Figure 4.1 Bedrock geology of study area with drill core sites A (SHEL 82-35), B (SABL 94-2) and C (TSZ 94-4) (yellow dots) over a length of 21.7 km along trend of the Tobeatic shear zone. Other drill holes in area marked in black (O'Neill and Poole 2016) and mineral occurrences (MOBD) in red (O'Reilly et al. 2016); map after White (2011) from online Geoscience Atlas (NS NRR). Highways in black.

4.1 Introduction

The kaolin occurrence within the Tobeatic Shear Zone is primarily hosted in a massive quartz-breccia, along the contact between the Davis Lake Pluton (SMB) leucomonzogranite and Goldenville Group metagreywacke. Three sites were selected from available drill cores along strike of the shear zone to the northeast (60 degrees) (Corey and Graves 1996) over a length of 21.7 km from the western site of Flintstone Rock (White Rock Property) - site A - to the eastern edge of Little Tobeatic Lake - site C (Fig. 4.1). The Tobeatic Shear Zone was delineated by ground VLF-EM and magnetic surveys by BP Resources Canada Ltd. in 1988 (McKenzie, 1988). Later through the use of the regional VLF-EM quadrature data, the shear zone was extended southwestward from the study area to a total length of >35km (Corey and Graves 1996).

4.2 Site A - Flintstone Rock - borehole SHEL 82-35 - Quartz and kaolin breccia

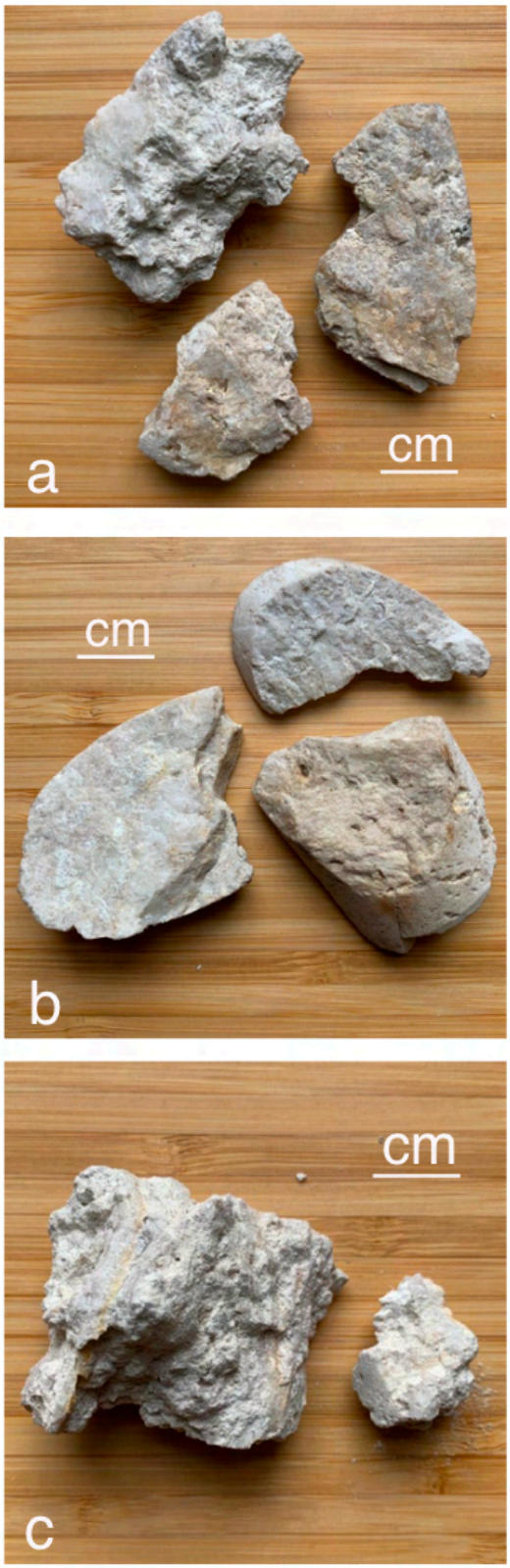

A 10 km long by ca.1.5 km wide zone of intense deformation containing both kaolin and silica was identified in 1980-1982 (Shell Canada Resources Ltd) as part of a regional exploration program. A series of boreholes were drilled to map out the mineral resource of quartz and kaolinite at Flintstone Rock (FR series), in subsequent years. The identified mineralized zone consists of a core of high-purity, brecciated quartz, with a varying thickness of 20 - 200 metres, pinching and swelling along strike and enveloped by quartz-kaolinite zones (MacGillivray and Shaw 2001a, 2001b).

Figure 4.2 Quartz breccia fragments broken along fractures, from vertical drill core SHEL82-35,
at depth of
a) 17 m (site A5); sample 35-17a and 35-17b
b) 53 m (site A3); sample 35-53a and 35-53b
c) 66 m (site A1); sample 35-66a and 35-66b

SHEL 82-35 is a vertical borehole, with 14.5 m of overburden, overlying 77 metres of the silificied, kaolinitized granite breccia, containing abundant kaolin (<50%) and kaolinized granitic clasts. The upper five meters of the silicious breccia are very altered (Fig. 4.2 a) with kaolinized sections of chalky feldspars and extensive fine-grained kaolinite-filled vugs. The following twenty five meters primarily contain massive quartz, with some sections showing textures evident of previous fracturing and resealing (Fig. 4.2b). Kaolinized zones are found throughout along fractures. At depths over 62 metres from surface, the rock alters to a clast-supported quartz breccia, hosting intense kaolinization (Fig. 4.2c) along a crosscutting stockwork network of quartz veins with vugs filled with clear prismatic quartz crystals. Fine-grained and coarser quartz veins, along with comb textures and vuggy interstitial spaces are suggestive of previous leaching and/or volume change. A succession of repeated brecciation and resealing by episodic silica flooding has been proposed (Corey and Graves 1996, Kontak and Kyser 2000).

4.3 Site B - Sabeans Lake - borehole SABL94-2 - pseudobreccia quartz stockwork vein

This site was initially drilled to investigate bedrock geology in areas of high airborne spectrometric anomalies proximal to the SMB contact, during exploration of the proposed extension of the Tobeatic shear zone (Corey and Graves 1996). Below four meters of overburden, drillcore SABL94-2 intersects the Goldenville metagreywacke; a massive, greenish-grey, fine- to medium-grained psammite interbedded with finer argillite, including hornfels with cordierite. Numerous vuggy quartz veins with anastomosing pattern as well as finer veins, corrugated and folded are found in association with a large quartz-breccia pipe, located between 45.3 to 102.1m of the core (Fig. 4.3).

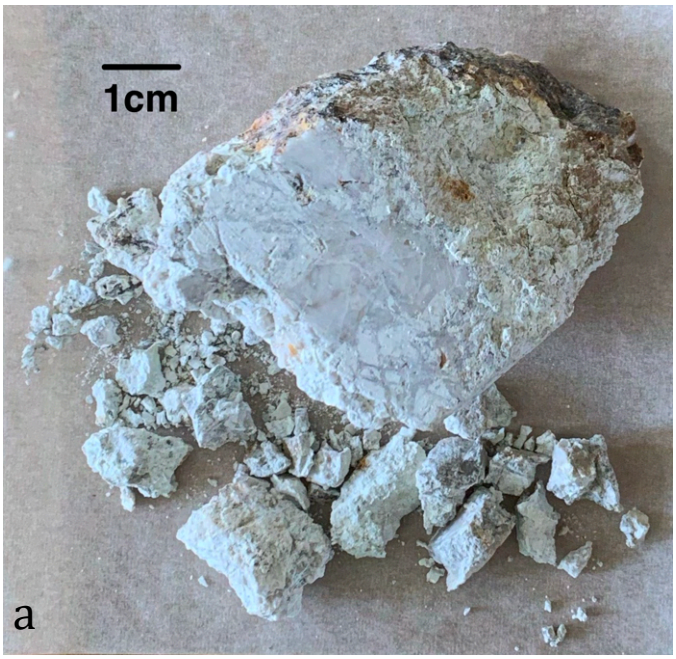

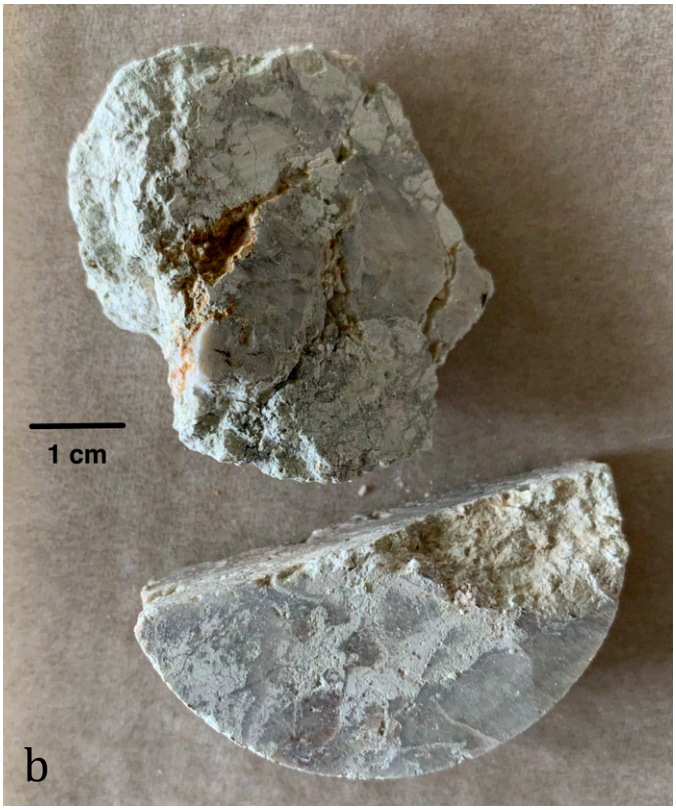

The over 50 m wide kaolinized zone was repeatedly fractured and resealed, with anastomosing quartz veins with vuggy fills and further cross-cut by abundant glassy to milky quartz veins. The kaolin is densely packed akin to a matrix. There is fracturing throughout with limonite staining. There are few remnants of the metagreywacke protolith. The core becomes increasingly fractured with depth and the abundant quartz veins increase in size. The zone may be described as a polyphase pseudobreccia, without a clear separation between the intensely kaolinized matrix and stockwork quartz veins, and a fluidized hydrothermal texture (Chauvet 2019).

Figure 4.3. Rock fragments from drill core SABL 94-2 of a ~50 m kaolin-quartz pseudobreccia in a metagreywacke protolith, at a depth of
a) 77m; sample SABL 11-1
b) 80m (site B2); sample SABL 10-1.

4.4 Site C - Little Tobeatic Lake - borehole TSZ 94-4 - multiple pathways of silica flooding

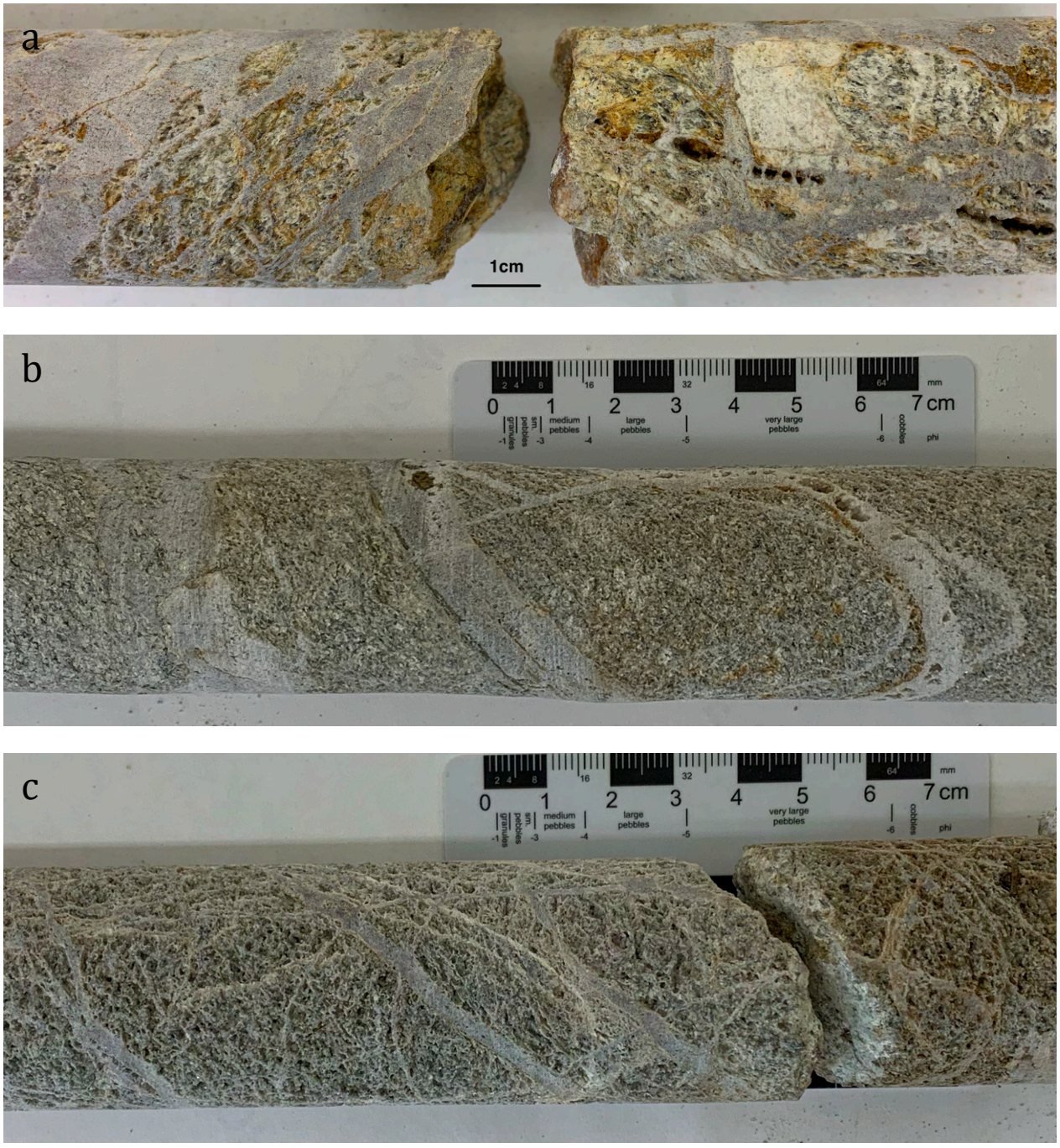

Figure 4.4. Kaolinized leucomonzogranite with a cross-cutting anastomosing network of quartz veins, from drill core TSZ 94-4, at core depth of a) 114 m (site C4); sample TSZ 17-1, b) 143 m; sample TSZ 22-1 and c) 161 m (site C2); sample TSZ25-1

The mapped contact between the Batholith and Meguma metasediments is between 1.7 to 2.6 km northwest of borehole TSZ94-4 and gravity data indicates extensive deformation along the contact in this area (Corey and Graves 1996). The top 60 m of the drill core, below three and a half metres of overburden till, consists of greenish grey metagreywacke, interbedded layers of massive, fine- to medium-grained psammite with pelite, including hornfels with cordierite. A localized shear band (Fig. 4.5) is intensely altered to ochre coloured clay below a narrow (<2cm) quartz band with ductile lineation; Over 10 m of quartz breccia underly the shear zone. Coarse-grained galena and sphalerite fill vugs or are disseminated, and fine-grained euhedral pyrite occurs as a late overgrowth. There is an intense zone, 2 m wide, of kaolinization at around 69 m, with quartz, either crystalline lining vugs or braided, cross-cutting veins, as well as hematization found throughout. As no hematized sections contain sulphides, it appears that hematization has leached and oxidized any sulphide minerals that might have been originally present (Corey and Graves, 1996). The jasper breccia is characterized by abundant (10–25%) fine grained, disseminated pyrite, while the jasper veins have a variable orientation and commonly crosscut preexisting quartz veins and mylonite bands. They, in turn, are crosscut and offset by milky and glassy quartz veins.

	Site A	Site B	Site C
Location	Flintstone Rock	Sabeans Lake	Little Tobeatic Lake
Borehole	SHEL 82-35	SABL 94-2	TSZ 94-4
UTM Coordinates (° 6) (zone 20)	N 4882126.41 E 294905.38	N 4883430 E 297710	N 4892310 E 313720
Azimuth / Dip	90 °	320 ° / -50 °	330 ° / -50 °
Total depth	91.4 m	182.8 m (140.03 m at 90 °)	174.7 m (133.83 m at 90 °)

Table 1.2 Borehole locations of drill cores used for rock samples along the Tobeatic Shear Zone.

4.5 Fluid-rock interactions

The quartz-kaolin mineralization found in the drill cores samples from the three boreholes along strike of the brittle-ductile Tobeatic shear zone (Table 1.2) indicate that oxidizing fluids were transported along interconnected pathways through both the leucomonzogranite and metagreywacke. The SW dipping shear band between the batholith and metasediment located below Little Tobeatic Lake (site C) and the fluidized pseudo-breccia textures within the Goldenville formation (site B) suggest initial syntectonic structural control (Chauver 2019). Overprinting and cross-cutting of quartz veins, with crystalline filled vugs, found in the breccia indicate that these zones are not representative of a single hydrothermal event but repeated flooding, brecciation and resealing along pre-established zones were periodically tectonically active for over 50 Ma (Corey and Graves 1996). The intense kaolinization associated with silica-flooding is restricted to discrete pathways (Fig. 4.5). It occurs along a single conduit (~50m) in borehole SABL 94-2 (site B) and as several anastomosing channels as in borehole TSZ94-4 (site C). The siliceous breccia intersected in borehole SHEL 82-35 (site A) is the widest section with around 95% SiO^2 and is found within a stratigraphic section of a quartz breccia enveloped by kaolinized breccia zones (10 — 40% kaolin). Polyphase quartz veins and resealing textures are abundant. Additional surveys conducted as part of Black Bull's explorations mapped a 700 to 800 metres long by 30 to 80 metres wide, mineralized zone at Flintstone Rock (MacGillvray 2000). Of the three borehole sites, SHEL 82-35 can be possibly interpreted as a tectonic trap, formed by differential shearing of the varyingly competent formations (Chauvet 2019), as shearing along the pathways created by hot circulating fluids stretched the rigid quartz bodies into a series of massive boudins (Shaw 2005). The pervasive brecciation includes microtectonic textures evident of both brittle cataclastic and ductile recrystallized fabrics (Passchier and Trouw 2005) (Fig. 4.6).

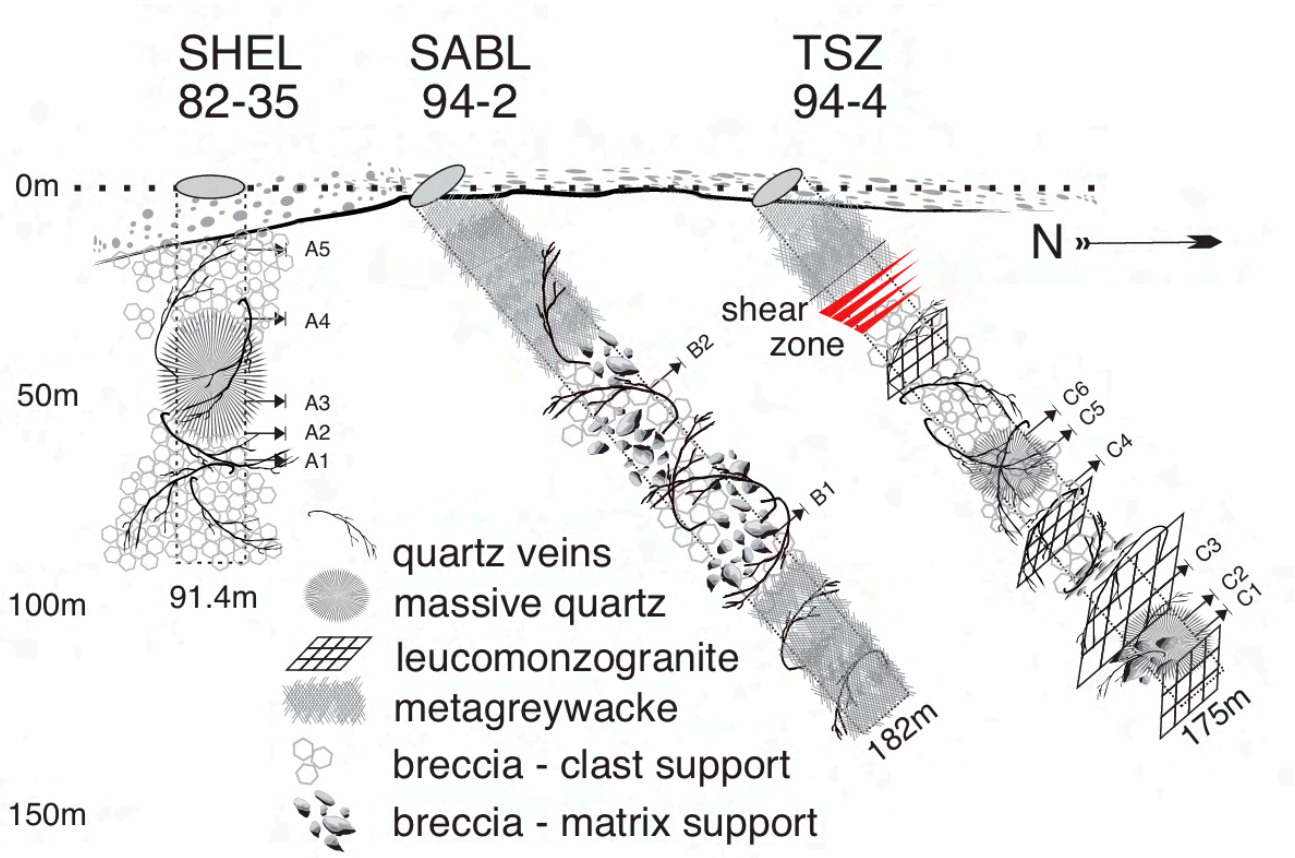

Figure 4.5 Sampled drill cores, with sampled sites identified. Refer to Appendix 1 for drill core log. Sample depth along core length: A1 - 66 m, A2 - 60 m, A3 - 53 m, A4 - 33 m, A5 - 17 m; B1 - 100 m, B2 - 80 m; and C1 - 165 m, C2 - 161 m, C3 - 150 m, C4 - 114 m, C5 - 104 m and C6 - 98 m.

Figure 4.6. Photomicrograph (XPL) of polished thin section from drill core SHEL 82-35, on following pages: a) A2 - SHEL-35-60b; cohesive polycrystalline quartz microbreccia, angular grains with straight grain boundaries and healed fractures. b) A1 - SHEL-35-66b; quartz-kaolin breccia. Angular to subangular quartz clasts, irregular quartz grain shapes and boundaries, cross-cutting vein displacement markers. Kaolin fills porosity (fuschia areas are voids), secondary biotite phase, healed fractures. Microtectonic textures with both cataclastic and dissolution-precipitation fabrics in both samples.

Legend: solid lines - micro fractures (fractures can be recrystallized with quartz, filled with kaolin, fluid pathway or show brittle deformation), dotted lines - brittle deformation with displacement, ellipse - euhedral recrystallized quartz; white hexagons - kaolin


a

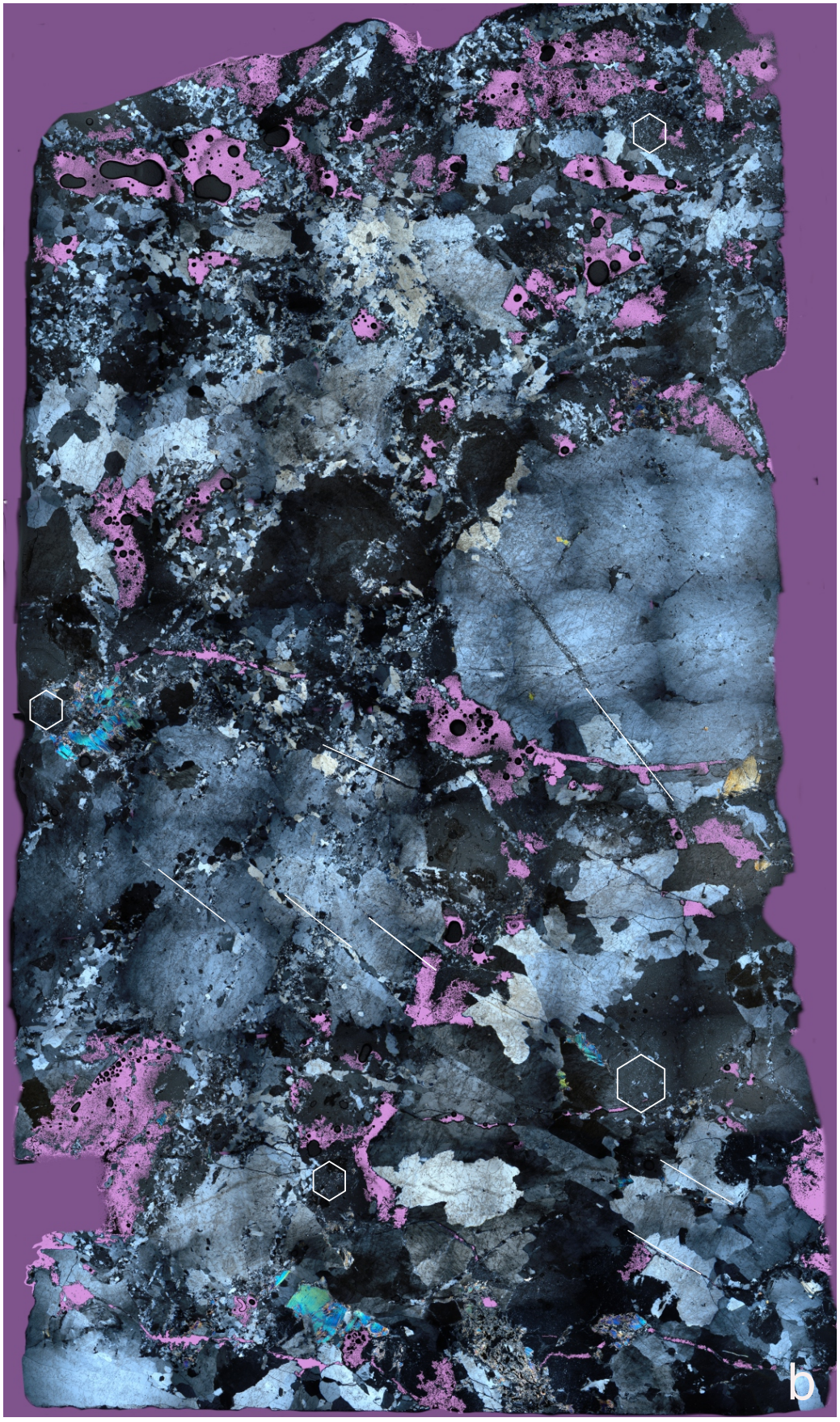
b

5: Petrographic characteristics of kaolin using SEM

5.1 Introduction

Authigenic kaolin crystals are ideally suited for scanning electron microscopy (SEM) because of their larger crystal size and well defined crystallinity (Bohor and Hughes 1970). The kaolin in this study was surveyed for its distinctive morphology, fabric and texture, growth mechanics, varying modes of occurrence, as well as mineral associations (Table 1.3 and Fig.5.1)

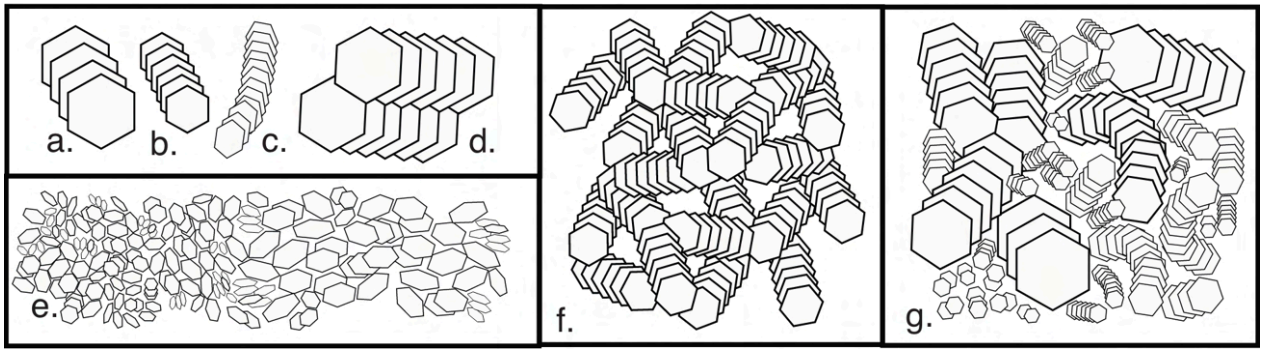

Figure 5.1 Diagram of distinct characteristics of kaolin identified using SEM images. Stacked booklets may be a) blocky, b) euhedral, c) vermicular, d) twinning by overlapping platelets. Stacked side-by-side; ranging to e) microcrystalline kaolin platelets stacked face-to-edge. Booklets can show various fabrics; f) porous 'card-house' aggregate or g) dense complex aggregates.

Fig.	*5.2*	*5.3*	*5.4*	*5.5*	*5.6*	*5.7*
	Morphology	Fabric and Texture	Growth Mechanics	Fractures and cavities	Veins and grain boundaries	Associations
a	(A1) SHEL-66b - SE - 1.3a	(A1) SHEL-66b - BSE - 1.5a	(A1) SHEL-66b - BSE - 1.3b	(A2) SHEL-60b - BSE - 3b	(A3) SHEL-53a - BSE - 4d	(A1) SHEL-66b - BSE - 1.2 g
b	(B2) SAB-11-1 - SE - 5	(B1) SAB-16-1 - BSE - 2d	(B1) SAB-16-1 - BSE - 1c	(B1) SAB-16-1 - BSE - 2c	(B2) SABL-11-1 - BSE - 3	(C5) TSZ-16-2 - BSE - 3d
c	(C4) TSZ-17-1 - BSE - 3e	(C5) TSZ-16-2 - BSE - 3c	(C5) TSZ-16-2, - BSE - 1i	(C5) TSZ-16-2 - BSE - 3a	(C2) TSZ-25-1 - BSE - 1a	(C1) TSZ-27-1 - BSE - 6c
d	(A1) SHEL-66b - SE - 1.1	(A3) SHEL-53a - BSE - 1g	(A2) SHEL-60b - BSE - 2c	(A5) SHEL-17b - BSE - 1g	(A1)SHEL-66b BSE - 2.2a	(A3) SHEL-53a - BSE - 4e
e	(B2) SAB-11-1 - SE - 5b	(B2) SAB-11-1 - BSE - 2e	(C2) TSZ-25-1 - BSE - 1e	(B2) SABL-11-1 - BSE - 3b	(B2) SABL-11-1 - BSE - 3a	(B1) SAB-16-1 - BSE - 2f
f	(C5) TSZ-16-2 - BSE - 1e	(C4) TSZ-17-1 - BSE - 4b	(C4) TSZ-17-1 - BSE - 3f	(C2) TSZ-25-1 - BSE - 2a	(C4) TSZ-17-1 - BSE - 4a	(C6) TSZ-15-1 - BSE - 2a

Table 1.3 Selected representative Scanning Electron Microscope (SEM) images from sites A-C; refer to figure 4.5 for location; see Appendix 2. Corresponds to figures 5.2 - 5.6; a - f

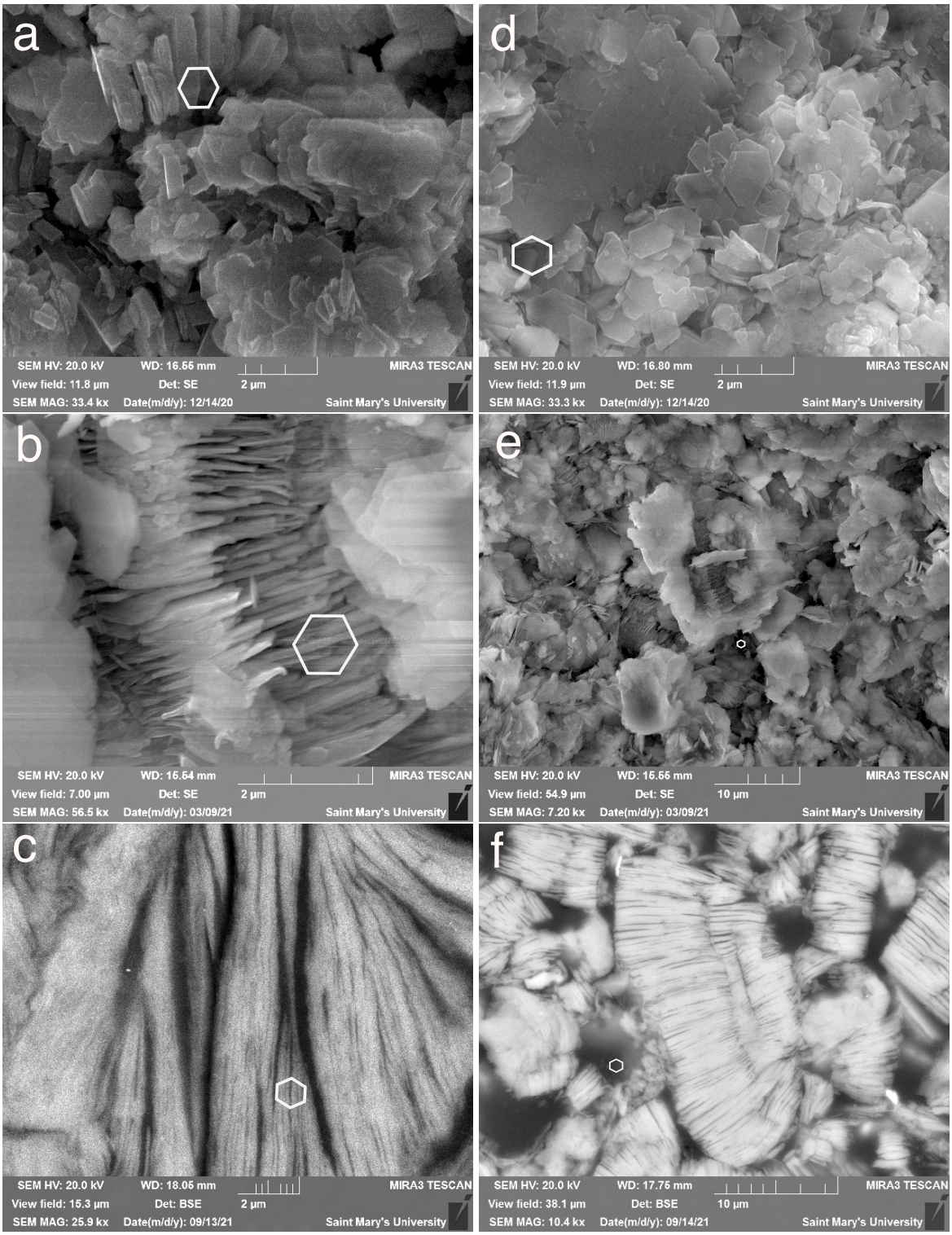

Figure 5.2 Back scatter electron (BSE) and secondary electron (SE) images representative of distinct kaolin morphologies: a) small size and aspect ratios, b) stacked kaolin booklets, with twinning, c) large aspect ratio and basal diameter, d) pseudo hexagonal crystals with face-to-edge plate growth, e) dense packing of booklets and plates f) kaolin booklet aggregate with porous 'card-house' structure. Refer to text for detailed description, table 1.3 and Appendix 2 for sample references. Hexagon = 1µm.

5.2 Morphology

The SEM images confirm a platy crystalline form of kaolin, with two distinct morphologies of a) hexagonal platelets that stack face-to-face (001) into booklets (Fig. 5-1 a - d) and b) microcrystalline pseudo hexagonal to subhedral particles, that can favour aggregating face-to-edge to form larger plates (Fig. 5.1 e). The size distribution along the basal plane ranges from <0.5 μm to >10 μm, with up to 2.5 μm circular diameter observed for the microcrystalline kaolin (Fig. 5.2 a and d). Overall the particle thickness, along prism plate, varies from transparently thin to blocky (>0.5 μm) and aspect ratios (diameter to thickness ratio) are estimated to range from 1 — 10 for a microcrystalline platelet (Fig. 5.2 d) and 10 to >60 for a hexagonal platelet in a booklet (Fig.5.2.f). There is an isolated example of extra-large platelets (Fig. 5.2 c), with aspect ratio upwards a hundred, and face-to-edge obliquely inter-grown laths of stacked kaolin, found at site C4 TSZ-17-1. Face-to-edge growth can be observed in microcrystalline size crystals, and can result in larger subhedral plates (Fig. 5.2 d). Kaolin booklets can be found inter-growing (akin to twinning) platelets with neighbouring booklets (Fig. 5.2 b) when stacking parallel side-by-side. Booklets, with stacking direction parallel to the c-axis, are the most common type of particle aggregation, and of fabric and texture. Compact booklets can arrange into dense masses, filled in with disordered subhedral plates of various orientations (Fig. 5.2 e). The three dimensional network of particles can alternatively arrange into a more porous structure, such as a 'card-house' aggregate (Fig. 5.2 f) with booklets edge-to-edge at various angles.

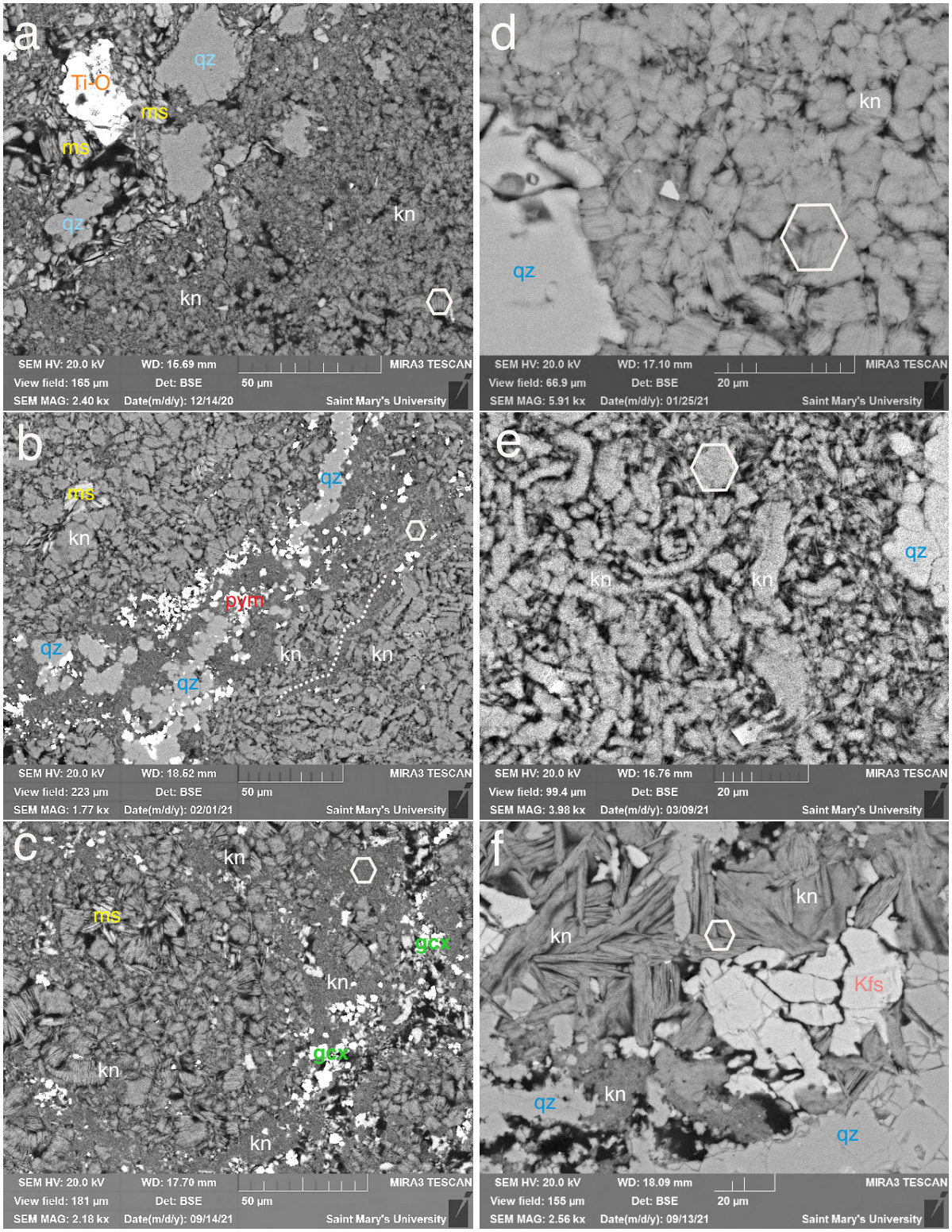

Figure 5.3 Back scatter electron (BSE) images of (a-c) kaolin aggregates of booklets and a dispersed microcrystaline matrix. Booklet stacks can be d) blocky, e) vermicular, or f) lath-like. Refer to text for detailed description, table 1.3 and Appendix 2 for sample references. Hexagon = 10µm.

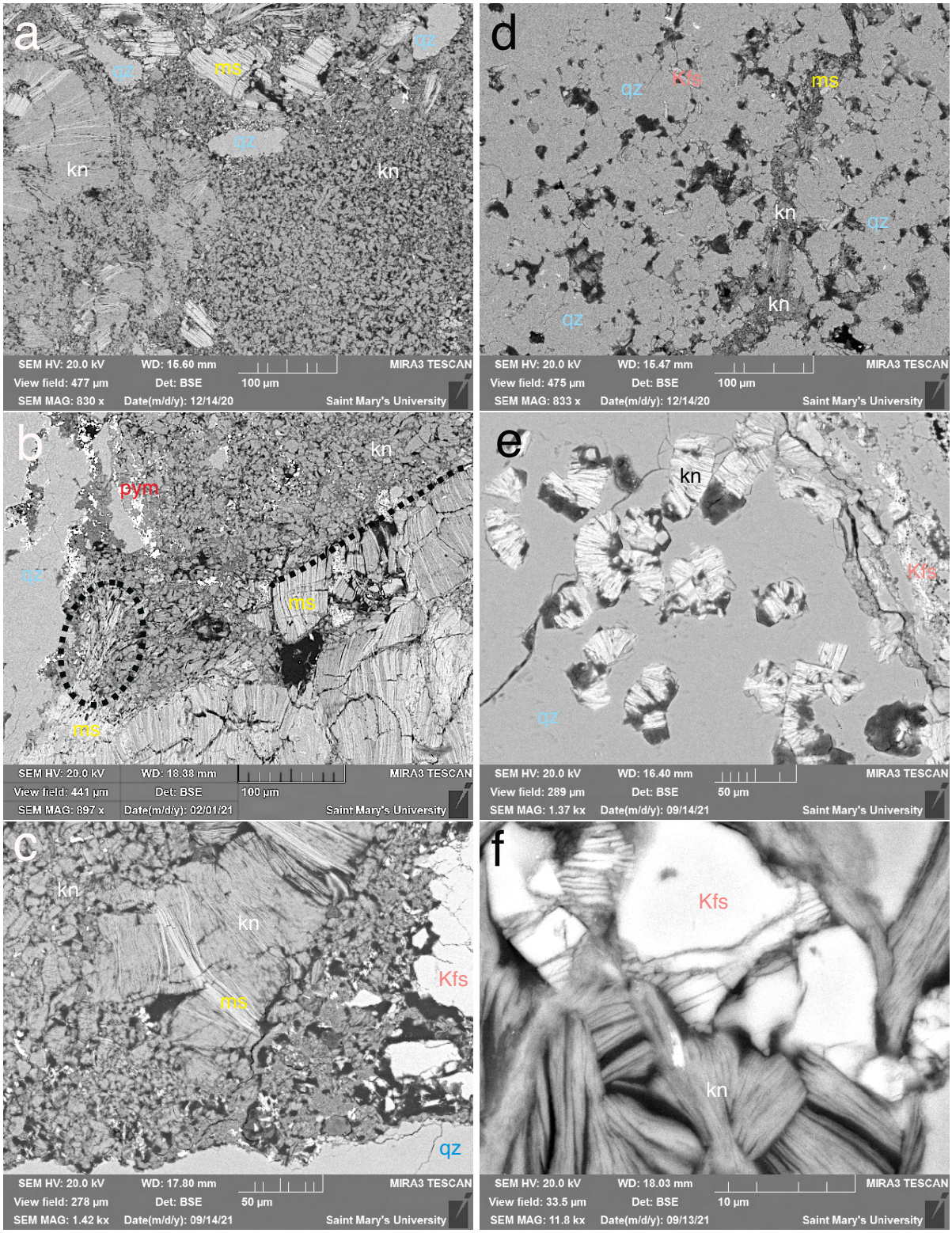

Figure 5.4 Back scatter electron (BSE) images of kaolin formation, a-c) replacement of mica; precipitation in quartz along d) grain boundaries and e) fractures;, and as (f) replacement of K-feldspar. Refer to text for detailed description, table 1.3 and Appendix 2 for sample references.

5.3 Fabric and Texture

The two distinct morphologies, of large euhedral booklets and a microcrystalline matrix can be found at all three sites (Fig. 5.3 a—c) in a range of fabrics, mainly depending on the type of aggregate structure. Orientation of the booklets directly affects the porosity of the network structure. The proportions of individual kaolin booklets can be found to be blocky (Fig. 5.3 d), vermicular (Fig. 5.3 e) or lath-like (Fig. 5.3 f). Microcrystalline kaolin can be found as the dominant morphology (Fig. 5.3 a), along discrete boundaries with booklets (e.g. white line on Fig. 5.3 b) or intermixed (Fig. 5.3 c); its orientation is typically disordered or dispersed. The lath-like kaolin, with a large size and aspect ratio, is arranged densly at oblique angles (Fig.5.3 f).

5.4 Alteration

Kaolin is found precipitated along grain boundaries with (Fig. 5.4 d), and filling fractures (Fig. 5.4 e) in quartz, of varied morphology and fabric. It can be associated with grain-size reduction by dissolution-reprecipitation of quartz (Fig. 5.4 d). Kaolin is predominantly formed from muscovite in all three boreholes, as follows: i) laminated within the phyllosilicate sheets of muscovite (Fig. 5.4 a), ii) as muscovite dispersed with kaolin (marked with black ellipse) (Fig 5.4 b), and iii) kaolin replacing muscovite sheets prior to decomposition of the grain, as a pseudomorph of muscovite (Fig 5.4 c). Distinct boundaries between some muscovite and kaolin (Fig. 5.4 b, partially marked with black line) are interpreted as remnant grain boundaries with disintegrated K-feldspar laths. It is inferred that most of the K-feldspar has been dissolved and only remnant K-feldspar crystals remain (Fig. 5.5 c—f) in the leucomonzogranite protolith. Kaolin has been found directly replacing K-feldspar (Fig. 5.4 f) in a Kfs vein, forming large lath-like stacks. The Kfs replacement by kaolin (Fig. 5.4 f) is unique in its occurrence and morphology.

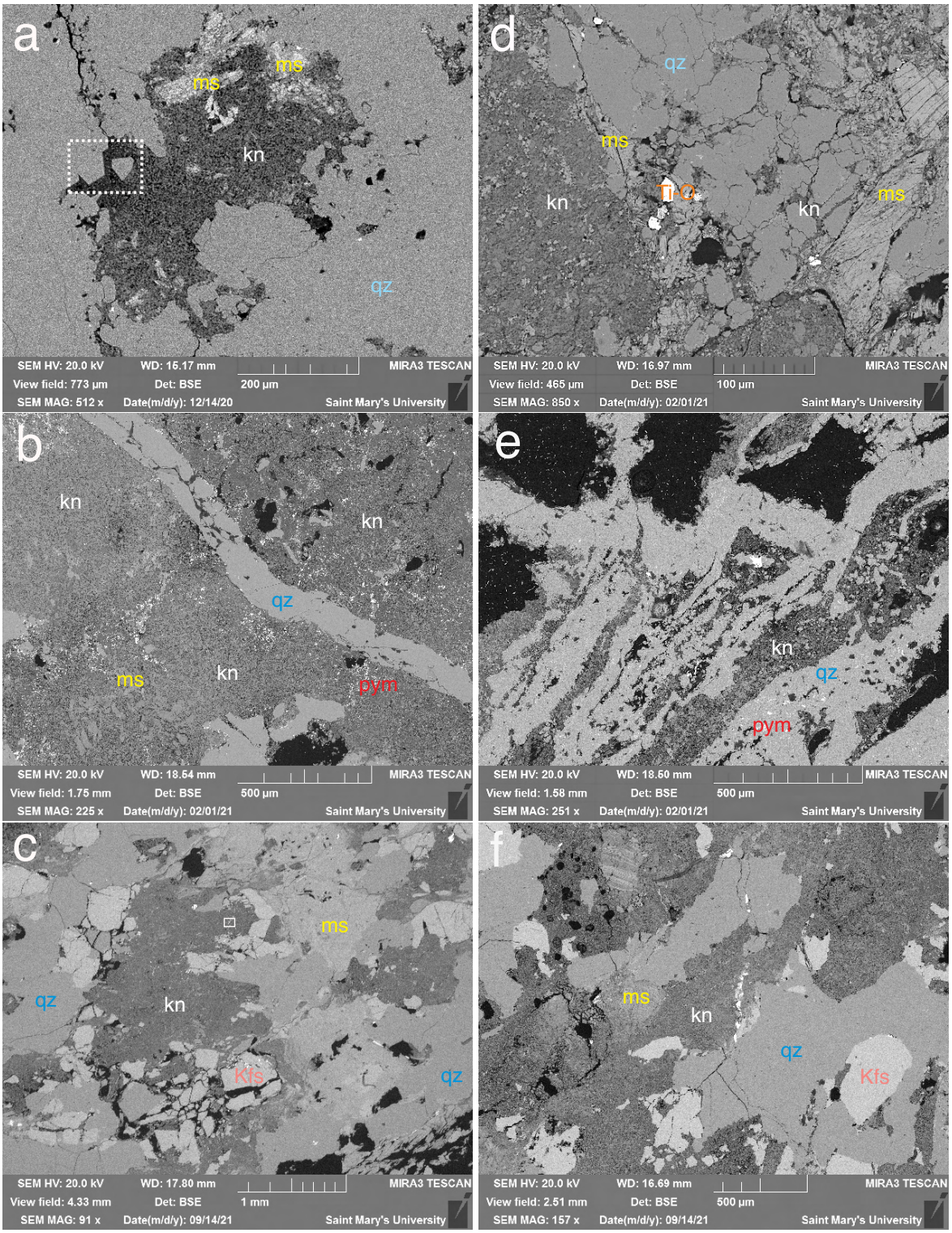

Figure 5.5. Back scatter electron (BSE) images of kaolin occurrence; a) filling vugs in massive quartz, b) as a matrix in pseudobreccia, c and f) argillic alteration of leucomonzogranite; e) with polyphase kinked and sheeted quartz veinlets. As well as filling fractures in quartz, d) cobweb texture. Refer to text for detailed description, table 1.3 and Appendix 2 for sample references.

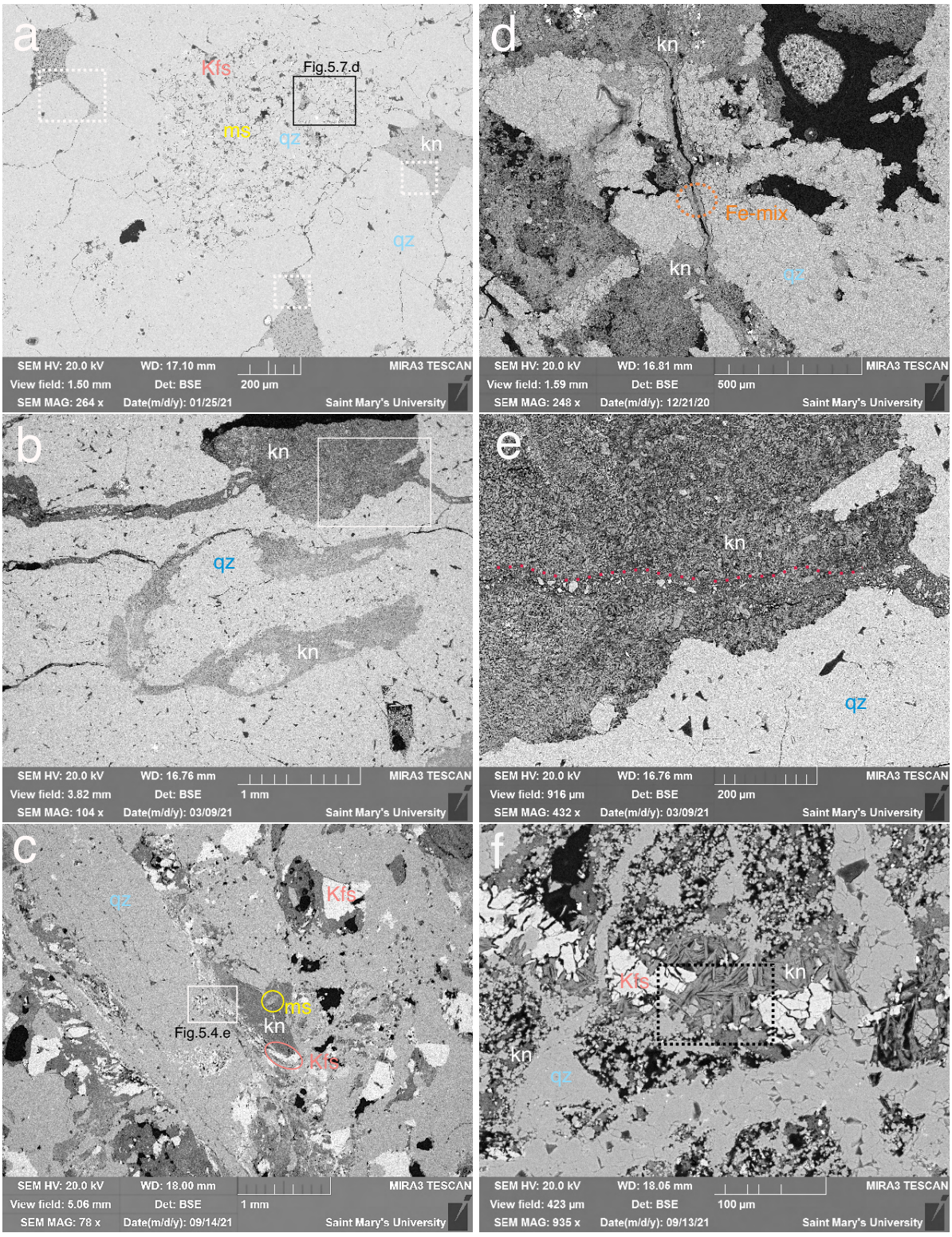

Figure 5.6. Back scatter electron (BSE) images of kaolin occurrence, a) along euhedral boundaries of recrystallized quartz and microbreccia; b and e) filling cavities and fractures in quartz pseudobreccia, c) in localized deformation band, d) subsequent kaolin veins in clast-supported breccia, f) replacement of K-feldspar. Refer to text for description, table 1.3 and Appendix 2 for sample references.

5.5 Occurrence

In the majority of the studied rock samples, quartz is the main component and it occurs as massive, veins or breccia. Kaolin primarily occurs with quartz. In the massive quartz found at Flintstone Rock, borehole SHEL 82-35, kaolin is distinctly found filling vugs (Fig.5.5 a) and along fine grained veins (Fig.5.4 d). Euhedral quartz grains of various size can be found in vugs filled with kaolin (Fig.5.5 a and Fig.5.6 a, shown with white rectangles). A microbrecciated texture can be seen in the polyphase quartz (5.6 a) with kaolin along grain boundaries; the quartz showing multiple phases of dissolution and precipitation. (Fig. 4.6 a). Some quartz grains form rings (Fig.5.7 d, shown with white circle) around a central area that is partly filled with kaolin, found at various scales in the microbreccia (Fig.5.6 a). The presence of voids in such areas suggest grain dissolution pores. In the clast supported breccia found at Flintstone Rock, borehole SHEL 82-35, kaolin is the dominant matrix with secondary mica, between the subangular to subround quartz sub grains (Fig.5.7 a). Various fractures, including cobweb texture (Fig.5.5 d) in quartz are filled with kaolin. A kaolin filled vein cross-cutting through quartz (Fig. 5.6 d) is inferred to be a later event; with kaolin dilating around a void as if insulating a wire, sometimes with remnants Fe-mix hydroxides found in the vein core. At Sabeans Lake, borehole SABL 94-4, kaolin occurs with polyphase anastomosing stockwork quartz veins, including kinked and sheeted veinlets (Fig.5.5 b and e). Kaolin occurs with secondary mica, filling fractures and cavities in the fluidized hydrothermal pseudobreccia. The quartz exhibits both shear and dilation, with brittle fractures and inter granular pores (Fig.5.6 b). There are remnants of transport of fine angular quartz crystal fragments along a dilation band in a larger kaolin filled cavity interconnected by fractures (Fig. 5.6 b and e). Argillic alteration of the leucomonzogranite at Little Tobeatic Lake, borehole TSZ 94-4, results in several modes of kaolin occurrence. Remnants of altered K-feldspar crystals

can be found throughout (Fig. 5.5 c and f), with the remnant crystals breaking apart into smaller blocks or being altered from the inside out to towards the grain boundary; leaving a kaolin-matrix fabric in its place. There are localized quartz deformation bands, with fine cataclastic K-feldspar alteration to kaolin (Fig. 5.6 c). A K-feldspar vein, cross-cut by quartz, is replaced by the large kaolin laths (Fig. 5.6 f). Polyphase anastomosing stock work quartz veins cross-cut and finely recrystallized "silica-sand" is found in the matrix along with kaolin (Fig. 5.6 f).

5.6 Mineral Association

The predominant mineralogy of the studied quartz-breccia includes quartz, kaolin, mica and remnant K-feldspar with minor albite. At Flintstone rock, borehole SHEL 82-35, the microbrecciated massive quartz is a finely crystallized mixture of qtz-kn-ms with accessory minerals including aluminum-phosphate sulphate (APS) mineralization of the Alunite supergroup (Jambor 1999), Table 1.6, with varying concentrations of Ba, Pb and Sr suggesting a Crandallite group mineral. Gorceixite is found in TSZ 94-4 (Fig. 5.7 c). Aluminum phosphate mineralization can be found in all three boreholes. Pyromorphite is found in both SHEL 82-35 and SABL 94-2 (Fig. 5.7 b and e). Precipitates of a microcrystalline sulfate rich mixture (Fig. 5.7 a and d) can also be found in the microbreccia at SHEL 82-35. Euhedral magmatic magnetite is found in massive quartz (Fig. 5.7 f) and barite is crystallized in voids of the jasper breccia in borehole TSZ 94-4. The many euhedral voids with remnants of sulphide minerals (e.g.. arsenopyrite) found in quartz reinforce the suggestion of prior leaching of sulphides, particularly in borehole SABL 94-4, while a single pyrite crystal is found in SABL 94-4.

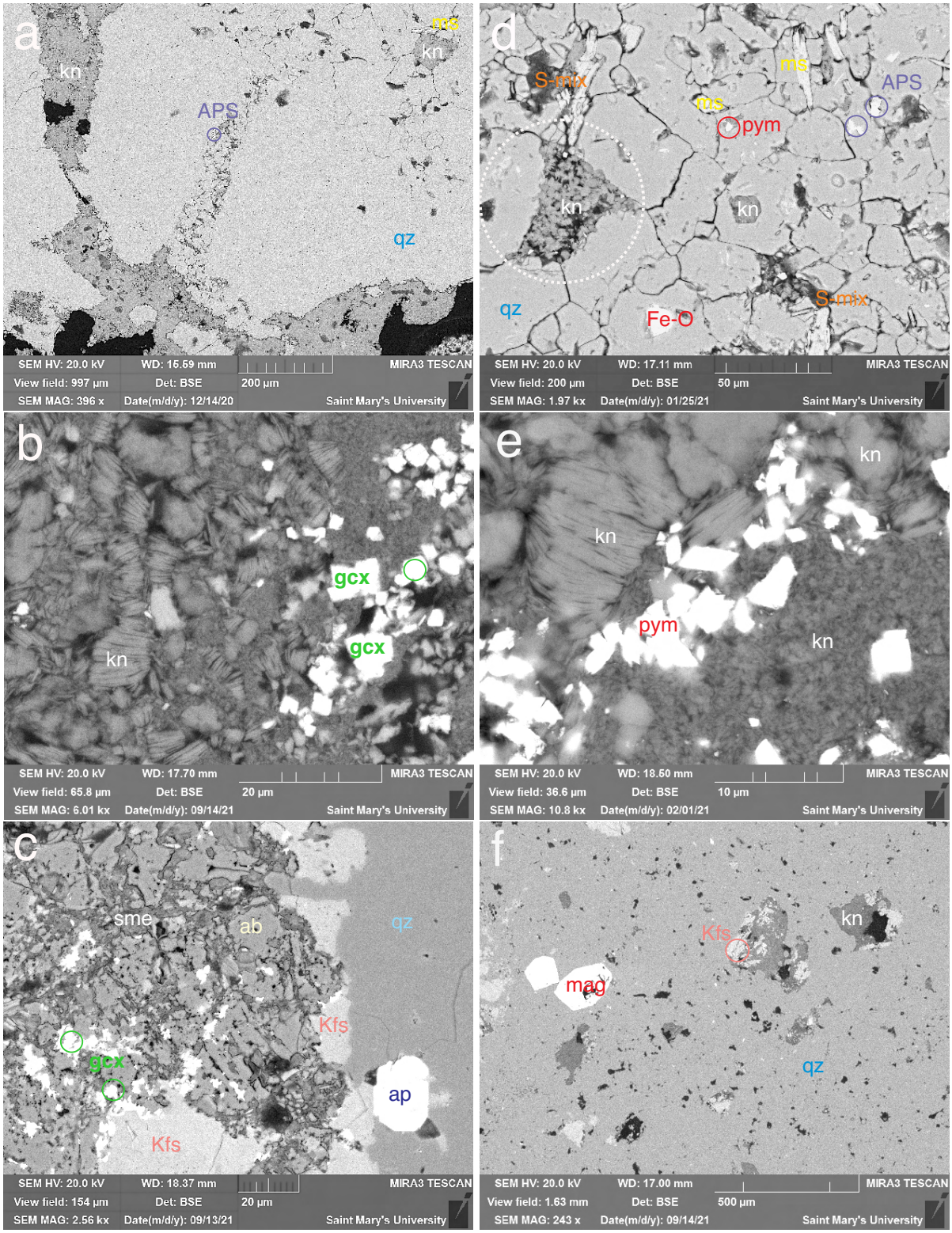

Figure 5.7. Back scatter electron (BSE) images of mineral association found at bore holes SHEL 35-82, SABL 94-4 and TSZ 94-4, including minerals of the crandallite group (APS), gorceixite (gcx), apatite (ap), pyromorphite (pym), magnetite (mag), and smectite (sme). Refer to text for detailed description, table 1.3 and Appendix 2 for sample references.

6: Geochemical analysis

6.1 Aluminosilicates

The predominant mineral assemblage of quartz-kaolin-mica was confirmed through EDS analysis. Kaolin EDS geochemical analysis shows two distinct formations, possibly two polymorph phases. Kaolin from borehole SABL 94-4 and TSZ 94-4 have SiO_2:Al_2O_3 (wt%) of 48.6 and 36.62 wt% and 48.5, 35.1 wt% respectively (Table 1.4). The kaolin from Flintstone Rock, SHEL 35-82 has excess SiO2, with an average wt% of 54.92. Notably, most of the kaolin sampled in SABL 94-4 and TSZ 94-4 includes FeO with an average wt% of 0.87 and 1.21 respectively; a limited number of samples have FeO in SHEL 82-35, with an average wt% of 0.45.

	Flintstone rock (SHEL 35-82)		*Sabeans Lake (SABL 94-2)*		*Little Tobeatic Lake (TSZ 94-4)*	
n	12		9		37	
wt%	SiO_2	Al_2O_3	SiO_2	Al_2O_3	SiO_2	Al_2O_3
Average	54.92	29.91	48.74	35.38	48.65	35.22
Range	54.3–55.5	29.2—30.2	48.1—50.4	33.0—36.9	47.7—50.8	33–36.7
Median	54.97	29.94	48.60	36.63	48.5	35.1
Mol. %	0.91	0.293	0.81	0.348	0.81	0.344
Si : Al ratio	**1.38**		**1.03**		**1.04**	

Table 1.4 Average silica and Alumina content of selected homogenous kaolin samples (samples with K not included), (*n*) number of analyses.

Muscovite is present in all three boreholes, with a higher K content at Flintstone Rock (SHEL 35-82), an average wt% of 13.28 compared to 8.91 wt% in SABL 94-2 and 8.67 wt% at TSZ 94-4 (Table 1.5). There appear to be at least two generations of Kfs crystallization at SHEL 35-82, an earlier remnant Kfs with comparatively high SiO_2 / low Al_2O_3 and a later fine grained

Kfs in quartz microbreccia with variable SiO_2 /Al_2O_3. Remnant leucomonzogranite K-feldspar in borehole TSZ 94-4 has an average K_2O wt% of 15.69; compared to 10.88 wt% in the finely crystallized K-feldspar found in SHEL 35-82 microbreccia in the massive quartz (Table 1.5). Remnant albite, probably altered from perthite, is found in TSZ 94-4 in association with smectite, not kaolin.

Avg. wt%	SiO_2	Al_2O_3	TiO_2	FeO	MgO	CaO	Na_2O	K_2O	Cl	*n*
Muscovite										
SHEL 35-82	51.30	25.30	0.53	2.99	1.16		0.35	13.42	0.02	*22*
range	48.97 54.73	22.68 27.86	0.00 1.04	1.35 6.55	0.67 1.64		0.00 1.85	10.37 15.72	0.00 0.32	
SABL 94-2	50.03	31.05		2.73	1.07			10.51		*4*
range	48.30 52.25	28.37 36.82		1.77 3.77	1.07 2.18			10.05 10.55		
TSZ 94-4	49.38	32.24	0.10	2.80	1.66		0.34	10.53		*6*
range	47.81 50.88	26.80 33.83	0.00 0.63	1.07 4.60	0.00 2.66		0.00 0.73	10.30 10.62		
Albite										
TSZ 94-4	69.09	18.89		0.28		0.28	11.45			*4*
range	68.76 69.59	18.72 19.08		0.00 1.13		0.00 0.41	11.05 11.88			
K-Feldspar										
SHEL 35-82	66.28	19.29	0.09	1.99	0.58		0.40	10.88		*6*
range	65.38 68.76	18.56 21.41	0.00 0.43	0.90 2.78	0.00 1.54		0.00 0.83	10.8 11.74		
TSZ 94-4	66.36	17.92		0.44			0.04	15.69		*40*
range	65.45 66.90	17.45 18.46		0.00 2.22			0.00 0.74	15.12 16.07		

Table 1.5 Average oxide chemical composition of analyzed muscovite and feldspar.
(*n*) number of homogenous looking crystals;
Muscovite LOI = assumed as 5%, Total = 100 wt%

6.3 Mineralization

Ti-oxides are found at all three sites, from euhedral grains (Fig. 5.5.d) to dispersed grains, and associated with muscovite. The TiO_2 mineral polymorph (Rutile, Anatase or Brookite) was not identified. The titania minerals are found most abundantly at Flintstone Rock in borehole SHEL 82-35, enriched with 2.49 — 4.58 wt% of Nb_2O_5 (Fig. 5.5.d). This is a relatively high concentration for titania the SMB, with average low - high Nb_2O_5 concentrations in wt% of 0.36 - 2.28 (Caruzzo et al. 2006). Rutile is typically identified as a common primary magmatic phase in the moderately to highly evolved rocks of the SMB (Caruzzo et al. 2006). At Flintstone Rock, Titania minerals can be also found associated with remnant, microcrystalline precipitates from siliceous (26 — 88 wt. % SiO_2) hydrothermal fluids, a few samples mineralized with Ni-Cu-Zn-Mo (<2 % wt%), and include a range of SO_3 from 2.36 — 17.78, with a median of 3.06. One euhedral pyrite is found in borehole SABL11-1 and barite filling voids in the jasper breccia in borehole TSZ 94-4. Euhedral magnetite (Fig 5.7.f) has been found in the jasper breccia with 1 wt% Zn and 3 wt% P_2O_5 (probably due to apatite inclusions). Euhedral apatite is also found in the jasper breccia (Fig. 5.7 c). Microcrystalline grains of Pb-Ba pyromorphite (Fig. 5.7 e) are found primarily dispersed in kaolin among quartz veins (Fig. 5.5 b) and filling voids in quartz (Fig. 5.5 e) throughout the pseudobreccia in borehole SABL 94-2 (Fig. 5.3 b), or in the finely crystallized in the quartz microbreccia in borehole SHEL 82-35 (Fig. 5.7 d). The aluminum-phosphate-sulphate (APS) are found finely crystallized in borehole TSZ 94-4 (Fig. 5.3 c), dispersed in micrycrystalline kaolin and directly associated with K-feldspar dissolution (Fig. 5.5 c - marked with white square - Fig. 5.7 b). Considering the Sr, Ba and Pb concentrations suggests a solid solution of goyazite-gorciexite-plumbogummite, part of the crandallite group (alunite supergroup) (Fig 5.6 a and Fig. 5.7 d).

	Aluminum phosphates			*Apatite*	*Sulfides*		*Amphibole*	*Oxides*		*Hydroxide*	*Hydrothermal*	
	crandalite	gorceixite	pyromorphite	apatite	pyrite	barite	antophyllite	magnetite	Ti-oxide	limonite	mixture	Zircon
n	*2*	*3*	*2*	*2*	*1*	*1*	*1*	*1*	*12*	*4*	*10*	*5*
SiO_2	1.75	1.98	5.34		9.51		47.76	2.28	1.93	17.37	52.44	28.51
Al_2O_3	24.07	28.24	26.68		4.43		4.35	2.97	0.73	9.69	7.01	2.11
TiO_2			0.56					0.65	97.46	0.85	0.39	
FeO	0.75	1.90	2.09		24.41		10.74	89.77	1.55	57.60	15.36	0.74
MgO	0.70	0.44					31.72				2.21	1.31
MnO							0.30					
CaO	3.30			48.49			0.88				2.47	0.91
Na_2O	0.43						0.77		0.81		2.72	
K_2O		0.44	0.38		0.31				0.44	0.67	1.20	
Nb_2O_5									3.06			
P_2O_5	31.56	30.50	28.05	44.77			0.77	3.27		1.68		
SO_3					61.33	37.24					5.40	
F	1.58	2.52		5.74							0.19	
Cl	0.33									0.79	1.57	
Co		0.12										
As_2O_3	0.18	0.02										
SrO	8.22											
BaO	11.74	24.27				62.94						
PbO	5.69	2.75	37.18									
Ni											0.06	
CuO											0.46	
Zn								1.05		0.28	0.21	
Sc_2O_3												0.13
ZrO_2												66.28
Assumed LOI	9.7	6.78					3.29			11.07	8.33	

Table 1.6 Average chemical composition of representative associated minerals analyzed with EDS (total = 100), (*n*) number of analyses.

6.4 Whole Rock Analysis

Oxide	wt%		*Element*	(ppm)		*Element*	(ppm)		*Element*	(ppm)		*Element*	(ppm)
SiO_2	79		Ba	1492		Ge	1		Pr	3.33		U	4.25
Al_2O_3	12.16		Be	2		Hf	1.9		Rb	180		V	16.5
Fe_2O_3	0.66		Ce	27.75		Ho	0.3		Sc	4		W	3.55
MnO	0.008		Co	1.6		La	11.35		Sm	3.35		Y	7.5
MgO	0.2		Cs	8		Li	27		Sn	9.3		Yb	0.7
CaO	0.05		Cu	5		Lu	0.13		Sr	114		Zn	100
Na_2O	0.08		Dy	2.1		Mn	53		Ta	1.35		Zr	61
K_2O	3.74		Er	0.9		Nb	7.8		Tb	0.4			
TiO_2	0.22		Eu	1		Nd	13.7		Th	9.55			
P_2O_5	0.17		Ga	20		Ni	30		Tl	0.95			
LOI	2.53		Gd	3		Pb	97.75		Tm	0.13			
Total	98.81											Nb / Ta	5.77
Rb / Sr	1.58		Ba / Sr	13.08		Li / Cs	3.36		Y / Th	0.78		Zr / Hf	32.11

Table 1.7 Chemical whole-rock major, minor and rare-earth element abundances for sample TSZ 94-4 17-2 using ICP OES / ICP MS, with elemental ratios Rb/Sr, Ba/Sr, Li/Cs, Y/Th, and Zr/Hf.

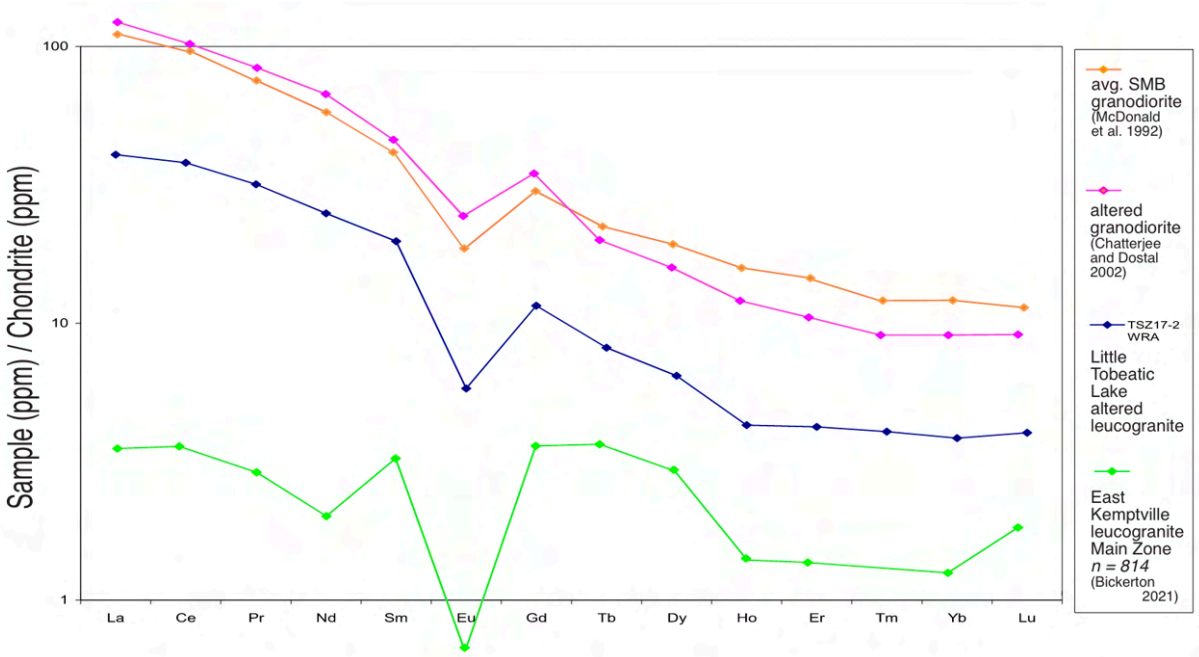

Figure 6.1. Spider diagram with rare-earth element (REE) concentrations normalized to chondrite for a) average SMB granodiorite (McDonald et al. 1992) and altered granodiorite (Chatterjee and Dostal 2002) b) Whole-rock sample from TSZ 94-4 sample 17-2 and c) East Kemptville leucogranite (ELK) Main Zone (Sn-W deposit) (Bickerton 2021). Chondrite normalized to McDonough and Sun (1995) and Boynton (1985).

The whole-rock REE elements for sample 17-2 from borehole TSZ 94-4 were determined for this project. Tis sample shows rare-earth element (REE) concentrations, normalized to chondrite (Boynton 1985), to have a comparable pattern to those of the grandiorite average of the South Mountain Batholith (SMB), though lower in magnitude. There is a depletion in HREE with (La/Yb) ratio of 16.2 and a distinct negative Eu anomaly. This depletion is pronounced on the spider diagram for the East Kemptville leucogranite from the mineralized (Sn-W) Main Zone, see Fig. 6.1. Sample 17-2 from borehole TSZ 94-4 represents the altered leucogranite host rock, and the mineralization is predominantly quartz, kaolin and altered K-feldspar, Figure 4.4. Observed depletion in Eu values, a function of feldspar fractionation, increases with alteration.

6.5. Stable oxygen isotopes - $\delta^{18}O$

sample		$\delta^{18}O$	$\delta^{18}O$ H_2O 100°C	$\delta^{18}O$ H_2O 150°C	$\delta^{18}O$ H_2O 200°C	$\delta^{18}O$ H_2O 250°C	$\delta^{18}O$ H_2O 300°C	$\delta^{18}O$ H_2O 350°C	$\delta^{18}O$ H_2O 400°C	$\delta^{18}O$ H_2O 450°C	$\delta^{18}O$ H_2O 500°C
1000 ln α	qtz <—> H_2O		23.4	16.4	11.5	8.1	5.6	3.8	2.5	1.5	0.8
SHEL 35-82 53	qtz-a3	7.7		-8.7	-3.8	-0.4	2.1	3.9	5.2	6.2	6.9
SHEL 35-82 60	qtz-a2	6.86		-9.54	-4.64	-1.24	1.26	3.06	4.36	5.36	6.06
SHEL 35-82 66	qtz-a1	5.45		-10.95	-6.05	-2.65	-0.15	1.65	2.95	3.95	4.65
1000 ln α	kln < — > H_20		15.3	10.0	6.4	4.0	2.3	1.1	0.3		
SHEL 35-82 66	kln-a1	7.61	-7.69	-2.39	1.21	3.61	5.31	6.51	7.31		
SABL 94-2 10-1	kln-b1	6.37	-8.93	-3.63	-0.03	2.37	4.07	5.27	6.07		
TSZ 94-4 17-2	kln-c1	6.47	-8.83	-3.53	0.07	2.47	4.17	5.37	6.17		
1000 ln α	qtz < — > kln			5.1	4.3	3.7	3.2				

Table 1.8 Analysed $\delta^{18}O$ values for quartz and kaolin samples, with calculated 1000 ln α and $\delta^{18}O$ H_2O at corresponding variable temperatures (Meheutt et al. 2007, Vho et al. 2020)

Three $\delta^{18}O$ values were obtained for kaolin, one from each of the three boreholes, and three $\delta^{18}O$ values for quartz from the borehole SHEL 82 - 35 at Flintstone Rock, see Table 1.1. The three quartz values are in the range of 5.45 — 7.7‰, which equilibrates with $\delta^{18}O$ H_2O values of -6.05 to 6.9 ‰ at temperature range of 200 — 500 °C, see Table 1.8. Below this temperature threshold, the values of $\delta^{18}O$ H_2O in equilibrium with quartz are too low. The three kaolin values are distinct, with $\delta^{18}O$ of 7.61 ‰ at SHEL 82 - 35 and a similar value of 6.37 — 6.47

from the two boreholes at Sabeans Lake and Little Tobeatic Lake. There is an apparent continuity between the two sites despite a 18 km distance. The three kaolin values equilibrate with δ ^{18}O H_2O values of - 0.03 to 5.31 ‰ at temperature range of 150 — 300 °C. The temperature may be as low as 100 °C if the kaolinite is formed solely from meteoric fluids.

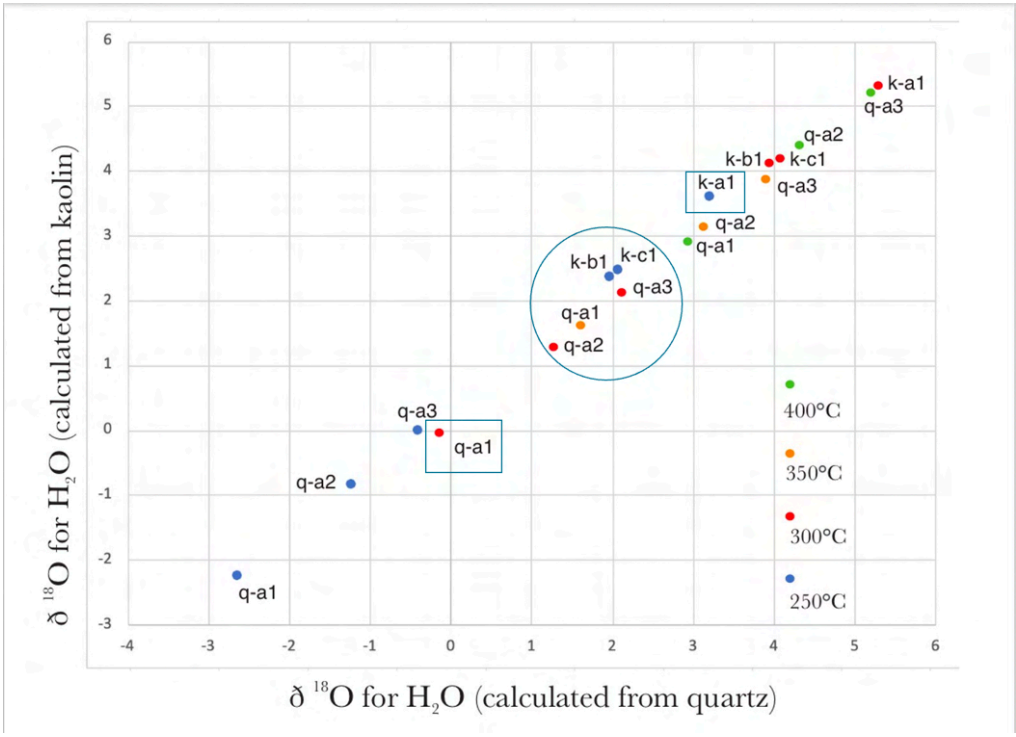

Figure 6.2 δ ^{18}O H_2O in equilibrium with kaolin and quartz samples in Table 1.8 at temperature range of 250-400°C; k - kaolin, q - quartz.

Comparing the values of δ ^{18}O H_2O in equilibrium with kaolinite and quartz, it is evident that the kaolin and quartz from sample from SHEL 82-35 were formed from isotopically distinct fluids (compare q-a1 with k-a1 on Figure 6.2) and they are not in isotopic equilibrium. Assuming a constant isotopic water composition, kaolin would have formed at ~235 °C if the quartz formed at 400 °C. The range in δ ^{18}O values for quartz is suggestive of a steep geothermal gradient -

assuming a δ ^{18}O H_2O value of ~2‰, q-a1 formed at approx. 300 °C., q-a2 at 320 °C and q-a3 at 365 °C over a span of less than 20 m - though considering the limited number of samples it is unlikely there is linear correlation. It is more plausible that the several generations of quartz, what is referred to as polyphase quartz in the SEM image annotations (Fig. 5.6 a and d) occurred intermittently. Considering the apparent isotopic disequilibrium between the kaolin and quartz, it is not possible to establish an overall temperature range of formation. It is therefore inferred that the quartz formed at higher temperatures than the kaolin, with up to a 100 °C temperature difference. The temperature gap widens with lower values of δ ^{18}O H_2O in equilibrium, so a higher temperature is assumed for kaolin to reconcile the difference. A constraint is offered by the δ ^{18}O values, whatever the formation temperature. The H_2O fluids in equilibrium with kaolin and quartz had an isotopic δ ^{18}O composition of < 6 ‰. Magmatic water in the SMB is in the range of >8 ‰ δ ^{18}O at 600 °C and metamorphic fluid is > 7.5 ‰ δ ^{18}O between 400 - 600 °C (Carruzzo et a. 2004, Kontak et al. 1987). It is well know that influxing meteoric water can lower the oxygen isotopes of altered rocks and ancient meteoric waters can have values down to -11.02 ± 0.43 $\delta^{18}O$ ‰ (Wei and Zho 2022).

The potential extended lifetime of the hydrothermal system limits kinetic constraints to no less than 100 Ma, see Figure 6.3. To better constrain fluid-rock interactions, general peleolatitude groups were identified in relation to tectothermal events. Distinct paleolatitudes were coordinated with a range of meteoric waters, which can be further constrained by elevation, at - 4.1 to -1.9 $\delta^{18}O$ ‰ at sea level, -3.3 to -7.9 $\delta^{18}O$ ‰ at an elevation of 1700 m, and -1.9 - 2.7 $\delta^{18}O$ ‰ at 1 km below, see Table 1.9.

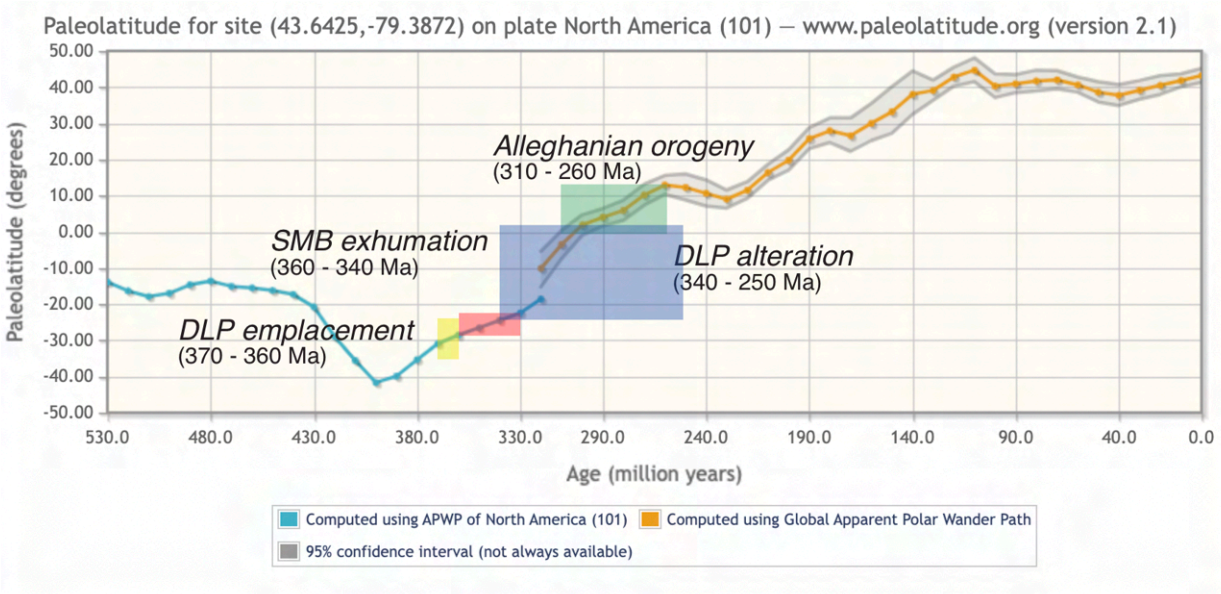

Fig 6.3 Paleolatitude for Halifax, Nova Scotia, divided into discrete events a) emplacement of the Davis Lake Pluton (in yellow), b) exhumation of the South Mountain Batholith (in red) c) alteration of the Davis Lake Pluton (in blue) and d) the Alleghanian orogeny (in green), (Douwe J.J et al. 2015).

latitude	-32 °S	-24 °S	-12 °S	0 °	12 °N
- 1000 m	0.3 $\delta^{18}O$ ‰	2.7 $\delta^{18}O$ ‰	1.5 $\delta^{18}O$ ‰	- 1.9 $\delta^{18}O$ ‰	- 1.8 $\delta^{18}O$ ‰
sealevel	-1.9 $\delta^{18}O$ ‰	0.5 $\delta^{18}O$ ‰	-0.7 $\delta^{18}O$ ‰	-4.1 $\delta^{18}O$ ‰	-4.1 $\delta^{18}O$ ‰
1700 m	-5.7 $\delta^{18}O$ ‰	-3.3 $\delta^{18}O$ ‰	-4.5 $\delta^{18}O$ ‰	-7.9 $\delta^{18}O$ ‰	-7.9 $\delta^{18}O$ ‰

Table 1.9 Precipitation water $\delta^{18}O$ ‰ isotope ratios for latitudes ranging from -32°S to 12°N (longitude is 0°), at sea level and elevation of 1700 m in modern conditions (Bowen & Wilkinson 2002).

7: Discussion

7.1 Kaolin characteristics and formation

The two common kaolin textures that have been observed: i) vermiform booklet aggregates and ii) finely crystalline are associated with expanded mica textures and feldspar dissolution, respectively (Psyrillos et al. 1998). The SEM images show kaolin as the main clay mineral (Table 2.1), exhibiting characteristic hexagonal booklet habit.

	Site A	**Site B**	**Site C**
Borehole	SHEL 82-35	SABL 94-2	TSZ 94-4
Polymorphs	unknown (inferred kaolinte + another phase)		
Morphology + Texture	densily packed blocky booklets + microcrystalline kn	complex aggregates, fine to vermicular kn booklets / microcrystalline kn discrete flow with qtz + pym + APS	dispersed booklets with microcrystaline kn (+ APS) / kn large-laths (altering Kfs)
Growth mechanics	kn dissolution + precipitation from ms / microbreccia with qz + Kfs + ms + APS	kn dissolution + precipitation from ms / kn along grain boundaries (inferred dissolved Kfs) / argillic alteration (Kfs + ms -> kn)	kn dissolution + precipitation from ms / remnant Kfs (dissolution) and kn replacement of Kfs / argillic alteration (Kfs + ms -> kn)
Occurrence	polyphase massive qz + qz microbreccia (grain boundary dissolution) / filling fractures + cavities (+ S-mix) / kn + Fe-mix veins in qtz subangular breccia / shear strain	precipitation in qz fractures and cavities (+ S-mix)/ volume reduction in qz /kn (>1mm) + qz veins (kinked and sheeted) / micro-crystalline kn dialation veins	leucogranite host / localized qz deformation bands (ductile + brittle) + kn vein and fracture filling / polyphase qz veins with dispersed qz + kn (dissolution + precipitation)
kaolin Si : Al ratio	**1.38**	**1.03**	**1.04**
Alumino - silicates	ms (K_2O 13.42 wt%) Kfs (K_2O 10.88 wt%)	ms (K_2O 10.51 wt%)	ms (K_2O 10.53 wt%) Kfs (K_2O 15.69 wt%) Ab (Na_2O 11.45 wt%)
$\delta^{18}O\ H_2O$	kn A - 200 °C 1.21 ‰ kn A - 250 °C 3.61 ‰ kn A - 300 °C 5.31 ‰	kn B - 200 °C -0.03 ‰ kn B - 250 °C 2.37 ‰ kn B - 300 °C 4.07 ‰	kn C - 200 °C 0.07 ‰ kn C - 250 °C 2.47 ‰ kn C - 300 °C 4.17 ‰

Table 2.1 Characteristics of kaolin in boreholes SHEL 82-35, SABL 94-2, TSZ 94-4

There is a second generation of finer kaolin mineralization that is quite prevalent, which may be a different kaolin phase; possibly halloysite or dickite. Halloysite can have a fine ground habit, while dickite is a higher temperature polymorph and can have large blocky, large booklets. Petrographically (i.e. SEM imagery), no halloysite with tubular morphology was found. Not having completed XRD analysis as part of this project has limited the identification of kaolin polymorphs.

7.2 Rock - fluid interactions

Previous research of hydrothermal deposits related to the South Mountain Batholith has interpreted mineral occurrences with characteristics resulting from of a mixture of fluids, based primarily on stable isotope and fluid inclusion studies (Kontak and Kyser 2000, Corey and Graves 1996, Caruzzo 2004). There are three possible fluid sources, magmatic, metasomatic/ metamorphic and meteoric (supergene) (Table 2.2).

	Hydrothermal fluids		
source	magmatic	metasomatic	meteoric influx
occurrence	quartz vein, tectonic fracturing	cooling granitic intrusion	fracture control, space filling features, mixing
structural / depth	faults and fractures	rock volume reduction	< 9 km
temperature / salinity / pH	exsolution ~ 600 °C (Carruzzo et a. 2004) med - high NaCl	~ 400-500 °C (Carruzzo et a. 2004)	higher fO_2 = oxidizing
mineral associations	Rutile (Ti-oxide) APS (P- enriched)	volatile rich	hematization, U, Mn
$\delta^{18}O$‰ whole-rock	10 ± 2 ‰ (Carruzzo et a. 2004)	15.4 ± 0.4 ‰ (Kontak et al. 2011)	3.6 ‰ (lowest) (Kontak et al. 1987)

Table 2.2 Characteristics of hydrothermal fluids associated with the SMB and Meguma Terrane

The stable isotopic chemistry of the SMB whole-rock has a documented uniform composition 10 ±2 ‰ (Caruzzo 2004) with only several lower $\delta^{18}O$ recorded - lowest 3.6 ‰ - interpreted to be as a result of supergene infiltration during late-stage crystallization (Kontak et al. 1987). Widespread disequilibrium is found in altered zones associated with greisens or pegmatites (Kontak et al. 1991). The metasomatic fluids from the Meguma supergroup have an average oxygen isotope value of 15.4 ± 0.4 ‰ (Kontak et al. 2011). The $\delta^{18}O$ values for quartz of 6.55 ± 1.15‰ in borehole SHEL 82-35 and 7.61, 6.42 ±.05 for kaolin, indicate that meteoric water must be a significant component in the formation fluids along the Tobeatic shear zone (Table 2.3).

The Devonian is characterized by major changes in ocean dissolved O_2 concentrations, producing marine anoxic events, with low $\delta^{18}O$ values (-8 ‰) (House 2022). High evaporation rates and warm temperatures were common during the period, with frequent sea level fall (regression) and rise (transgression). The Upper Kellwasser extinction event, separating the Frasnian and Famennian Stage (373.2 - 358.0 Ma) of the Late Devonian is associated with a dramatic decrease in dissolved oxygen levels within oceans (House 2022). It is possible that the study area was below the water table in the saturated zone during time of formation. Association of alteration with fractures has been repeatedly noted (Chatterjee and Dostal 2002), increasing the depth of water infiltration. It is expected that the $\delta\ ^{18}O\ H_2O$ may have also partially equilibrated with the metasediments of the Goldenville formation, as hydrothermal pseudobreccia passes directly through the metasediments, in borehole SABL 82-35.

Distinct and variable, positively correlated, temperatures and salinities have been identified in borehole TSZ 94-4, with quartz formation as low as 100 °C to > 300 °C, and < 5 wt% to >20% NaCl respectively, including magmatic hydrocarbons (Kontak and Kyser 2000,

Corey and Graves 1996). The Nb/Ta (5.77) whole rock ratio from TSZ 94-4 is within the range of the MPG (muscovite-bearing peraluminous granite) magmatic-hydrothermal alteration (Ballouard et al. 2020).

	$\delta^{18}O$ ‰		
range	- 8 to - 4	**- 4 to 0**	0 to 4
paleolatitude	0 ° to 12 °N sealevel -12 °s to 12 °N 1700m	0 - 12 °N -1000m **-32 °S - 12 °N sealevel** -12 °S - 12 °N 1700 m	- 32 °S to -12 °S - 1000m +

Table 2.3 Association of $\delta^{18}O$‰ with paleolatitude, refer to table 1.9

The measured $\delta^{18}O$ values for quartz and kaolin are lower than previously documented $\delta^{18}O$ values at Flintstone rock, in in range of >9 ‰ (Kontak and Kyser 2000). The variability is interpreted as formation at different times and conditions (i.e. temperature and depth). Mineralogically distinct generations of kaolinite and quartz have been previously noted to be present at Flintstone Rock (Kontak and Kyser 2000). The three measured kaolin values equilibrate with $\delta\ ^{18}O\ H_20$ values of - 0.03 to 5.31 ‰ at temperature between 200 — 300 °C, with a difference of 1.25 ‰ between the three borehole sites. The kaolin found in the matrix of the subangular quartz breccia, at a depth of 66m in borehole SHEL 82-35, is not in equilibrium with the accompanying quartz clasts. It is also distinct from that formed at Sabeans Lake (SABL 94-2) and Little Tobeatic Lake (TSZ 94-4), which could be reconciled as a temperature gradient between the three sites with a magmatic heat source in vicinity of Flintstone Rock. A potential source of exsolving magmatic fluids could have been the Wedgewood pluton or the smaller intrusions along the SE boundary of the shear zone. Generally $\delta^{18}O$ values increase with higher

formation temperatures and/or depth. Magmatic water content and fO2 are unknown and oxidiation potential is uncertain. Generally, melts that are more enriched in water (>4 wt%) and with a high oxidation state (>FMQ + 1.3–2) are critical factors for generation of not only Au mineralization (Bao et al. 2018) but also kaolin. These factors were not analysed to constrain the influence of magmatic fluids.

7.3 Relative chronology

It is assumed that magmatic fluids remained in circulation at Flintstone Rock (borehole SHEL 83-35) during the late-stage crystallization and uplift of the SMB (~370 - 350 Ma) and reactivated during protracted igneous activity, such as the neighbouring mantle-derived Wedgeport pluton (U-Pb zircon age of 316 ± 5 Ma) (Shellnutt and Dostal 2019, Cormier et al 2011). Lamprophyre dykes in the Wedgeport pluton have yielded $^{40}Ar/^{39}Ar$ hornblende ages between 231 - 222 ±3 Ma (Pe-Piper and Reynolds 2000). Mineralization of kaolin and quartz in the study area may have occurred intermittently over a span of 100 Ma, with siliceous magmatic fluids mixing with heated supergene fluids. The open-space comb texture found in quartz veins in the altered granite at Little Tobeatic Lake (borehole TSZ 94-4) (Fig. 4.4) suggest a later formation at shallower depths (< 1km), in line with proposed epithermal models (Corey and Graves 1996).

7.4 Localized genetic model

It is inferred that a magmatic source of fluid and heat at Flintstone Rock was reactivated periodically over >100 Ma, in several episodes between 360 - 220 Ma. Previous work at Flintstone Rock by Kontak and Kyser (2000), as well as Corey and Graves (1996) had reported

fluid mixing in the formation of the kaolin / quartz deposit along the Tobeatic shear zone. It has also been previously noted that the quartz and kaolin were not deposited in equilibrium with each other. This project supports the previous findings but the lower $\delta^{18}O$ indicate a more significant proportion of supergene fluids.

The kaolin breccia zones at Flintstone Rock appear to be deformation bands with shear related disaggregation along a steeply dipping strike-slip fault zone, and dissolution - precipitation controlled by periodic influx of siliceous magmatic fluids. Further, considering the inferred low confining pressures, it is plausible that Flintstone Rock is an extension fissure along the contact of the Davis Lake Pluton and the Meguma Group. It is noted that the brittle-plastic transition occurs at higher temperatures under extension than contraction. If the formation of quartz and kaolin occurred during the uplift of the South Mountain Batholith, a variation textures related to pressure should be observed through additional review of available core logs. Volume reduction in quartz (borehole SABL 94-2) and open-space comb texture (borehole TSZ 94-4) both suggest rapid decompression. The low pressure determined by fluid inclusion isochores from Flintstone Rock (max. P of ca. 1.2 - 2.7) support interpretation of an open and connected fracture network (Kontak and Kyser 2000).

It may be possible that a higher temperature fluid migrated laterally along the pathways of the contact between the Davis Lake Pluton and the Meguma Supergroup. There is a consistent $\delta^{18}O$ value constraining kaolin formation SABL 94-2 and TSZ 94-4, despite the 17 km distance and varying host rock (metasediment and leucogranite). A clear origin of fluids at Little Tobeatic Lake has not been reconciled with previously calculated variable temperatures and salinity that seemingly lack a magmatic source.

Conclusion

The quartz-kaolin deposit at Flintstone rock is rare in its occurrence in the Meguma Terrane. The mineral resource reports describe it as a steeply-dipping zone of kaolinized granite, seven to eight hundred meters in length by 30 to 80 m wide (Shaw 2005), Fig.3.1. The resource evaluation identifies nearly twenty million tonnes of high-grade (avg. 97% SiO_2) quartz and seven million tonnes of kaolinized granite (Shaw 2005). Classified as a breccia-type mineral occurrence (MacDonald 2001), its initial geological formation could be of tectonic origin during emplacement and uplift of the SMB and potentially active protractively for >100Ma.

Formation of the quartz-kaolin deposit appears structurally controlled by a complex of fault planes, shear bands, extension fissures and growing network of fractures during rapid decompression of the igneous intrusion. There is inferred to have been an intermittent source of oxidizing siliceous magmatic fluids, such as the Wedgewood pluton or other small intrusions, that significantly mixed with supergene fluids during uplift. The $\delta\ ^{18}O\ H_20$ of the supergene fluids is estimated to be between -4 to 0 ‰ at sealevel and the study area is assumed to be in the saturated zone with fluid infiltration structurally controlled.

The kaolin formation at Flintstone Rock (SHEL 82-35) is interpreted to pre-date the kaolin formation further NE along the Tobeatic shear zone, as observed in boreholes SABL 94-2 and TSZ 94-4. The macroscopic open-space textures in the quartz coincide with previous interpretations of formation in a shallow, epithermal setting. Petrographic and geochemical analysis indicate that all three sites along the Tobeatic shear zone are connected spatially but require further evaluation to clearly understand the kaolin formation, during an extensive time period of > 100 Ma of intermittent hydrothermal and tectonic activity.

References

Bao X., Yang L., He W., Gao X. (2018) Importance of Magmatic Water Content and Oxidation State for Porphyry-Style Au Mineralization: An Example from the Giant Beiya Au Deposit, SW China. Polymetallic Metallogenic System: special issue. *Minerals* 8(10)

Ballourd C., Massuyeau M., Elburg M.A, Tappe S., Viljoen F., Brandenburg J.T. (2020) The magmatic and magmatic-hydrothermal evolution of felsic igneous rocks as seen through Nb-Ta geochemical fractionation, with implications for the origins of rare-metal mineralization. *Earth-Science Reviews*. v.203

Benn K., Roest W.R., Rochette P., Evans N.G. and Pignotta G.S., (1999) Geophysical and structural signature of syntectonic batholith construction: the South Mountain Batholith, Meguma Terrane, Nova Scotia, *Geophysical Journal International* v.136 pp.144-158

Bethke C.M., Farrell B., Sharifi M. (2022) GWB Essentials Guide. Aqueous Solutions LLC. Illinois, US https://www.gwb.com/pdf/GWB2022/GWBessentials.pdf

Beaudoin, G & Therrien, P. (2004) The web stable isotope fractionation calculator. In: Handbook of stable isotope analytical techniques, Volume-I. De Groot, P.A. (ed.). Elsevier: 1045-1047.

Beaudoin, G & Therrien, P. (2009) The updated web stable isotope fractionation calculator. In: Handbook of stable isotope analytical techniques, Volume-II. De Groot, P.A. (ed.). Elsevier: 1120-1122.

Bickerton, L. (2021) Geological, fluid-chemical and petrochronological studies of the East Kemptville Sn (-Cu-Zn-Ag-In) deposit and its Devonian host batholith (Nova Scotia, Canada). PhD Thesis. Laurentian University, Sudbury, Ontario, Canada.

Bohor B.F., Hughes R.E. (1970) Scanning electron microscopy of clays and clay minerals. *Clays and Clay Minerals*, 18 (1970), pp. 7-23.

Boynton W. V. (1984) Geochemistry of the rare earth elements: meteorite studies. In Rare Earth Element Geochemistry (ed. P. Henderson), pp. 63–114. Elsevier

Bristow C.M. and Exley, C.S. (1994) Historical and geological aspects of the china clay industry of southwest England. *Transactions of the Royal Geological Society of Cornwall*, 21. 247-314

Carruzzo S., Clarke D.B., Pelrine K.M, Macdonald M.A. (2006) Texture, composition, and origin of rutile in the South Mountain Batholith, Nova Scotia. *The Canadian Mineralogist* 44(3) pp.715-729

Carruzzo S. Kontak D.J., Clarke D.B., Kyser T.K. (2004) An integrated fluid-mineral stable-isotope study of granite-hosted mineral deposits of the New Ross Area, South Mountain Batholith, Nova Scotia, Canada: Evidence for Multiple Reservoirs. *The Canadian Mineralogist* v.42 pp.1425-1441

Corey, M.C., Graves, R.M., (1996) Investigation of epithermal-type, breccia-hosted Pb-Zn-Ba-Au mineralization within the Tobeatic shear zone of southwestern Nova Scotia; Nova Scotia Department of Natural Resources, Minerals and Energy Branch, Open File Report ME 96-008, p1-81

Corey, M.C., (1988). An occurrence of metasomatic aluminosilicates related to high alumina hydrothermal alteration within the South Mountain Batholith, Nova Scotia. *Maritime Sediments and Atlantic Geology*, 24, pp.83-95

Chauvet, Alain. (2019). Structural Control of Ore Deposits: The Role of Pre-Existing Structures on the Formation of Mineralised Vein Systems. *Minerals*. v.9(56)

Chatterjee A.K., Dostal J., (2002) Deep drill hole in the Devonian South Mountain batholith, Nova Scotia: a potential for hidden deposits within the batholith. *Atlantic Geoscience* 38(1)

Chatterjee A.K., Kontak D.J., (1992) The East Kemptville tin deposit, Yarmouth County, Nova Scotia: a Pb-isotope study of the leucogranite and mineralized greisens-evidence for a 366 Ma metallogenic event. *Canadian Journal of Earth Sciences,* vol.29, p.1180-1196

Chatterjee A.K, Cormier, R.F. (1991) A Rb-Sr geochronological study of the Davis Lake pluton, South Mountain batholith, southern Nova Scotia: evidence for a 374 Ma time of emplacement. Mines and Minerals Branch Report of activities, part A. Nova Scotia Department of Natural Resources Report.

Clayton, R. N., and Mayeda, T. (1963) The use of bromine pentafluoride in the extraction of oxygen from oxides and silicates for isotopic analysis. *Geochimica et Cosmochimica Acta*, v. 27, pp. 47-52.

Cormier R., Keppie J., Odom L., (2011) U–Pb and Rb–Sr geochronology of the Wedgeport granitoid pluton, southwestern Nova Scotia. Canadian Journal of Earth Sciences. 25. p255-261.

Dill, H.G. (2016) Kaolin: Soil, rock and ore: From the mineral to the magmatic, sedimentary and metamorphic environments. *Earth-Science Reviews*. v.161 pp16-129

Dill, H.G. (2003) A comparative study of APS minerals of the Pacific Rim fold belts with special reference to South American argillaceous deposits. Journal of South American Earth Sciences. 15:5 p.301-320

Dostal J., Chatterjee A.K., (2009) Lead isotope and trace element composition of K-feldspars from peraluminous granitoids of the Late Devonian South Mountain Batholith (Nova Scotia, Canada): Implications for petrogenesis and tectonic reconstruction. *Contributions to Mineralogy and Petrology,* vol.159, p.563-578

Dostal J., Chatterjee A.K., Kontak D.J., (2004) Chemical and isotopic [Pb, Sr] zonation in a peraluminous granite pluton: origin by crystal-fluid fractionation. *Contributions to Mineralogy and Petralogy,* vol.14, p.74-90

Dostal J., Chatterjee A.K. (1995) Origin of topaz-bearing and related peraluminous granites of the Late Devonian Davis Lake pluton, Nova Scotia, Canada: crystal versus fluid fractionation. *Chemical Geology*. v.123 pp.67-88

Douma, M. (1978) Gravitational interpretation and modelling of South Mountain batholith, Nova Scotia. Unpublished B.Sc. thesis. Dalhousie University, Halifax, Nova Scotia.

Douwe J.J. van Hinsbergen, Lennart V. de Groot, Sebastiaan J. van Schaik, Wim Spakman, Peter K. Bijl, Appy Sluijs, Cor G. Langereis, and Henk Brinkhuis (2015) A Paleolatitude Calculator for Paleoclimate Studies (model version 2.1)

Duncan P.M., Kohlsmith R.L., Wells S.G., (1982) Report of Diamond Drilling on Mineral Exploration Licenses 4122 and 4124. East Kemptville Project. Yarmouth Co., Nova Scotia. Shell Canada Resources Ltd.

Dominy S., Camm G.S. (1998) Geology and hydrothermal development of the Bostraze-Balleswidden kaolin deposit, Cornwall, UK. Applied Earth Science IMM Transactions section B. v107 pp.148-157

Dutrow B., Klein C. (2007) The manual of mineral science. 23rd ed. John Wiley & Sons, New Jersey, US.

Ece O.I., Sans B.E., Esenli F. (2009) Hydrothermal alteration and origin of the kaolin-alunite deposits: Duvertepe district, Simav Graben, Turkey. Conference Paper: 46th Annual Meeting of the Clay Minerals Society, Montana USA.

Fulgignati P. (2020) Clay Minerals in Hydrothermal Systems. *Clays, Clay Minerals and Geology* 10 919, pp1-17

Gardolinski de Costa, J.E.F. (2005) Interlayer Grafting and Delamination of Kaolinite. Doctoral Thesis. Christian-Albrechts-University; Kiel, Germany.

Geoscience Atlas, Nova Scotia Natural Resources and Renewables https://fletcher.novascotia.ca/DNRViewer/?viewer=Geoscience

Giles P.S. (1985) A major post-Viséan sinistral shear zone-new perspectives on Devonian and Carboniferous rocks of southern Nova Scotia; in *Guide to Granites and Mineral Deposits of southwestern Nova Scotia*, eds. A. K. Chatterjee and D. B. Clarke; Nova Scotia Department of Mines and Energy, Paper 85-3, p. 233-264.

Guggenheim S., Alietti A., Bain D.C. Drits V.A., Formos M.L.L., Galan E., Hundall W., Koster H.M., Paquet H, Watanabe T., (1996) Report of the Association Internationale Pour l'Etude Des Argiles (AIPEA) Nomenclature Committee for 1996. Clays and Clay Minerals 32(3):493-495

Halter W.E., Williams-Jones A.E., Kontak D.J. (1998) Origin and evolution of the greisenizing fluid at the East Kemptville tin deposit, Nova Scotia, Canada. Economic Geology v.7 pp.1026-1051

Ham L.J., Macdonald M.A. (1991) Preliminary Geological Map of Wentworth Lake (21A/04); Nova Scotia Department of Mines and Energy, Open File Map 91-0200, scale 1:50000

Hannon P., Roy D. (2005) Resource Report for the White Rock Quartz, Kaolin and Mica Deposit. MineTech International Limited, Halifax, Canada

Hedenquist J.W., Arribas A., Gonzales-Urien E. (2000) Exploration for epithermal gold deposits. In: Hagemann S.E., Brown P.E. (Eds) Rev Econ Geol. 13: 245 - 277

Hohn S., Frimmel H.E., Pasava J. (2014) The rare earth element potential of kaolin deposits in the Bohemian Massif (Czech Republic, Austria). *Mineralium Deposita*; Heidelberg 49:8 p.967-986

Horne R.J., King M.S., Kontak D.J., O'Reilly G.A. and Black D. (2005) The Kemptville Shear Zone: Regional Shear Related to Granite Emplacement and Mineralization. *Mineral Resources Branch, Report of Activities 2005. Nova Scotia Department of Natural Resources,* Report ME 2006-1, p. 19-37

Horne R.J., MacDonald M.A., Corey M.C. and Ham L.J. (1992) Structure and emplacement of the South Mountain Batholith, southwestern Nova Scotia. *Atlantic Geology,* vol.28, p.29-50

Horne R.J., Corey M.C., Ham L.J. and MacDonald M.A. (1988) Primary and secondary structural features in the eastern portion of the South Mountain Batholith, southwestern Nova Scotia: implications for regional stress orientations during intrusion. *Marine Sediments and Atlantic Geology*, 24, pp. 71-82

House M. R. (2022) "Devonian Period". Encyclopedia Britannica, 15 Oct. https://www.britannica.com/science/Devonian-Period. Accessed 16 December 2022.

Jambor J.L. (1999) Nomenculture of the Alunite Supergroup. *Canadian Mineralogist*. v.37 pp.1323 - 1341

Keppie J.D., Keppie D.F., Dostal J. (2021) The northern Appalachian terrane wreck model. *Canadian Journal of Earth Sciences*. v.58 pp.542-553

Keppie J.D., Krogh T.E., (2000) 440 Ma igneous activity in the Meguma Terrane, Nova Scotia, Canada; part of the Appalachian overstep sequence? *American Journal of Science, vol.300(6), p.528-538* *https://novascotia.ca/natr/meb/data/pubs/bull07/Bull07.pdf*

Keppie J.D. (1992) Structure of the Canadian Appalachians. *Mines and Energy Branches, Nova Scotia Department of Natural Resources.* Bulletin 7, p1-97

Kontak D.J, Horne R.J., Kyser K. (2011) An oxygen isotope study of two contrasting orogenic vein gold systems in the Meguma Terrane, Nova Scotia, Canada, with implications for fluid sources and genetic models. *Mineralium Deposita* v.46(3) pp. 289-304

Kontak D.J., Ansdell K., Dostal J., Halter W., Martin R., Williams-Jones A. (2001). The nature and origin of pegmatites in a fluorine-rich leucogranite, East Kemptville Tin Deposit, Nova Scotia, Canada. *Earth and Environmental Science Transactions of the Royal Society of Edinburgh,* vol.92(2), p.173-200

Kontak D.J., Kyser K. (2000) Preliminary Fluid Inclusion and Oxygen Isotope Studies of the Flintstone Rock (NTS21A/04) silica-clay Deposit, Yarmouth County, Nova Scotia. *Report of Activities,* p.37-48

Kontak D.J., Cormier R.F., Reynolds P.H., Taylor K. (1991). Preliminary results of Rb/Sr and $^{40}Ar/^{39}Ar$ geochronological investigations, East Kemptville leucogranite, southwestern Nova Scotia: Evidence for ca. 370 Ma age of emplacement and multiple tectono-thermal overprinting events. In Mines and Minerals Branch Report of Activities 1989, Part A Nova Scotia Department of Mines, Report 89-3, pp.41-47

Kontak D.J., Cormier R.F. (1991) Geochronological evidence for multiple tectono-thermal overprinting events in the East Kemptville muscovite-tapaz leucogranite, Yarmouth County, Nova Scotia, Canada. *Canadian Journal of Earth Sciences*. v.28 pp.209-224

Kontak D.J., Kerrich R., Strong D.F. (1991) The role of fluids in the late-stage evolution of the South Mountain Batholith, Nova Scotia: further geochemical and oxygen isotopic studies. Atlantic Geology 27 pp.29-47

Kontak D.J., Strong D.F., Kerrich R. (1987) Crystal-melt+fluid phase equilibria versus late-stage fluid-rock interaction with granitoid rocks of the South Mountain Batholith, Nova Scotia: Whole Rock Geochemistry and Oxygen Isotope Evidence. *Marine Sediments and Atlantic Geology*, v. 24 pp. 97-110

Liu J., Xia QK., Kuritani T., Hanski E., Yu, H-R. (2017) Mantle hydration and the role of water in the generation of large igneous provinces. *Nature Communications,* vol.8

MacDonald L.A., Barr S.M., White C.E., Ketchum J.W.F. (2011). Petrology, age, and tectonic setting of the White Rock Formation, Meguma terrane, Nova Scotia: Evidence for Silurian continental rifting. *Canadian Journal of Earth Sciences*, vol.39(2), p.259-277

MacDonald M.A. (2001) Geology of South Mountain Batholith, Southwestern Nova Scotia. Open File Report 2001-2. *Nova Scotia Natural Resources, Minerals and Energy Branch.* https://novascotia.ca/natr/meb/data/pubs/01ofr02/01ofr02_Chapter00.pdf

MacDonald M.A., Home R.J., Corey M.C., Ham L.J. (1992) An overview of recent bedrock mapping and follow-up petrological studies of the South Mountain Batholith, southwestern Nova Scotia, Canada. *Atlantic Geology*, vol. 28(1), p.7-28

MacGillivray G.T., Shaw W.G. (2000) Kaolinite, Silica, Flintstone Rock, Yarmouth County, Nova Scotia. Report on Prospecting, Geological Mapping, an IP/Resistivity Survey, and Drilling and Drill Core Chemical and Physical Analyses [Report of Work, the Yarmouth Quartz - Kaolinite Project, January 1, 1999 to December 31, 1999, Mineral Licenses 3009, 3009A, 2428, 2429, 2431, 3486] ME2000-037 p1-405

MacGillivray G.T., Shaw W.G. (2001a) Silica, Flintstone Rock, Yarmouth County, Nova Scotia. Report on the Bulk Sampling Program, Yarmouth Quartz - Kaolinite Project, October 1 to December 1, 2000. Mineral Licences 3009, 2009A, 2428, 2431, 3486. *Black Bull Resources Incorporated*. ME2001-033 p1-26

MacGillivray G.T., Shaw W.G. (2001b) Quartz, Kaolinite, Flintstone Rock, Yarmouth County, Nova Scotia. Report on the Diamond Drilling, Yarmouth Quartz - Kaolinite Property, October-November, 2000. Mineral Licences 3009, 2429. *Black Bull Resources Incorporated*. Assessment Report ME2001-041 p1-50

MacGillivray G.T., Shaw W.G. (2001c) Quartz, Kaolinite, Flintstone Rock, Yarmouth County, Nova Scotia. Report on Induced Polarization Survey, Mineral Licenses: 2428, 2429, 3486. *Black Bull Resources Incorporated*. Assessment Report ME2001-042 p1-96

Mawer C.K., White J.C. (1987) Sense of displacement on the Cobequid-Chedabucto fault system, Nova Scotia, Canada. Canadian Journal of Earth Sciences v.24(2) pp. 217-223

Méheut M, Lazzeri M, Balan E, Mauri F (2007) Equilibrium isotopic fractionation in the kaolinite, quartz, water system: Prediction from first-principles density-functional theory. Geochimica et Cosmochimica Acta 71: 3170-3181.

McDonough W.F., Sun S.S. (1995) The composition of the Earth. *Chemical geology*, 120, p. 223-53.

McKenzie C. B. (1988) Report on till geochemistry, prospecting and geophysics, Tobeatic Lake property; BP Resources Canada; Nova Scotia Department of Mines and Energy, Assessment Report 88 - 295

McNeil N.C. (2019) The mineralogy, petrography, and paragenesis of the polymetallic (Co-Ni-As-Au) veins of the Nictaux Falls Dam Occurrence, Annapolis Valley, Nova Scotia. Undergraduate thesis, B.Sc. Geology. Saint Mary's University, Halifax NS

Moore D.M., Reynolds R.C. (1997) *X-Ray diffraction and the identification and analysis of clay minerals.* 2nd ed. Oxford University Press, Oxford.

Murphy J.B., Keppie J.D. (2005) The Acadian Orogeny in the Appalachians. *International Geology Review*, vol. 47, p. 663–687

O'Reilly, G.A., Demont, G.J., Poole, J.C., and Fisher, B.E. (2016) DP ME 002, Version 11, 2016, Nova Scotia Mineral Occurrence Database; Nova Scotia Department of Natural

Resources, Geoscience and Mines Branch, Digital Product DP ME 002.
O'Reilly G. (1992) Petrographic and geochemical evidence for a hypogene origin of granite-hosted, vein-type Mn mineralization at the New Ross Mn deposits, Lunenburg County, Nova Scotia, *Canada. Economic Geology*, vol.87, p.1275-1300

O'Reilly G.A. (1992) Granite- and metasediment-hosted mineral deposits of southwestern Nova Scotia; Geological Association of Canada-Mineralogical Association of Canada, Joint Annual Meeting, Wolfville '92, Field Trip C-3 Guidebook, 91p.

O'Reilly G.A., Farley E.J., Charest M.H. (1982) Metasomatic-hydrothermal mineral deposits of the New Ross - Mahone Bay Area, Nova Scotia. Paper 82-2. Department of Mines and Energy. Nova Scotia. pp. 1-96.

Owen J.V., Greenough J.D., Hy C., Ruffman A. (1988) Xenoliths in a magic dyke at Popes Harbour, Nova Scotia: implications for the basement of the Meguma Group. *Canadian Journal of Earth Sciences.* vol.25(9), pp. 1464-1471

Parkhurst D.L., (1995) User's Guide to PHREEQC - - a Computer Program for Speciation, Reaction-Path, Advective-Transport, and Inverse Geochemical Calculations. Water-Resources Investigations Report 95-4227. U.S. Geological Survey (https://wwwbrr.cr.usgs.gov/projects/GWC_coupled/phreeqc.v1/)

Passchier C.W., Trouw R.A.J. (2005) "Deformation Mechanisms." In Microtectonics, ch.3 pp25-56. Springer, Berlin.

Pe-Piper G. and Reynolds P.H. (2000) Early Mesozoic alkaline dykes, southwest of Nova Scotia, Canada, and their bearing on Triassic-Jurassic magmatism. *Canadian Mineralogist*, 38, 217-232.

Poppe L.J, Paskevich V.F., Hathaway J.C. Blackwood D.S (2001) A Laboratory Manual for X-Ray Powder Diffraction. *United States Geological Survey*, Open File-Report 01-041.

Psyrillos A., Manning D.A.C., Burley S.D. (1998) Geochemical constraints of kaolinization in the St. Austell Granite, Cornwall, England *Journal of the Geological Society, London,* vol. 155, p.829-840

Shaw W.G. (2005) White Rock Property Yarmouth County, Nova Scotia; Assessment Report for Exploration License No. 05531 (NTS 21-A-04). Black Bull Resources Ink. AR 2005-067

Shellnutt J.G., Owen J.V., Yeh MW. (2019) Long-lived association between Avalonia and the Meguma terrane deduced from zircon geochronology of metasedimentary granulites. *Scientific Reports* v.9:4065

Shellnutt J.G., Dostal J. (2019) Derivation of the Early Carboniferous Wedgeport pluton by crystal fractionation of a mafic parental magma: a rare case of an A-type granite within the Meguma terrane (Nova Scotia, Canada). *Cambridge University Press*. 157(2), 248-262

Shellnutt J.G., Dostal J. (2012) An evaluation of crustal assimilation within the Late Devonian South Mountain Batholith, SW Nova Scotia. *Geological Magazine*

Schmidt, G.A., G. R. Bigg and E. J. Rohling (1999) "Global Seawater Oxygen-18 Database - v1.22" https://data.giss.nasa.gov/o18data/

Wei, C.-S., Zhao Z.-F. (2022). Paradoxically lowered oxygen isotopes of hydrothermally altered minerals by an evolved magmatic water. *Science Rep*. 12(1)

Waldron J.W.F., Barr S.M., Park A.F., White C.E., Hibbard J., (2015) Late Paleozoic strike-slip faults in Maritime Canada and their role in the reconfiguration of the northern Appalachian orogen. *Tectonics*, vol.34(8), p.1661-1684

Walker S.A., Azetsu-Scott K., Normandeau C., Kelley D.E., Friedrich R., Newton R., Schlosser P., McKay J.L., Abdi W., Kerrigan E., Craig S.E., Wallace D.W.R (2015) Oxygen isotope measurements of seawater: A comparison of cavity ring-down spectroscopy (CRDS) and isotope ratio mass spectrometry (IRMS). *Limnology and Oceanography Methods* v.14(1) pp.31-38

Wilson I.D, Keeling J. (2016) Global occurrence, geology and characteristics of tubular halloysite deposits. *Clay Minerals* v.51 pp.309-324

White C.E., Horne R.J., Ham L.J., MacDonald M.A. (2012) Bedrock geology map of the Wentworth Lake area, NTS sheet 21A/04, Digby, Shelburne and Yarmouth counties, Nova Scotia; Nova Scotia Department of Natural Resources, Mineral Resources Branch. Open File Map ME 2012-087, scale 1:50 000

White C.E. (2010). Stratigraphy of the Lower Paleozoic Goldenville and Halifax Groups in Southwestern Nova Scotia. *Atlantic Geology*

Vho A, Lanari P, Rubatto D (2020) An Internally-Consistent Database for Oxygen Isotope Fractionation Between Minerals. Journal of Petrology 60:2101-2129

Yuan,Y., Shi G., Yang M. et al. (2014) Formation of a hydrothermal kaolinite deposit from rhyolitic tuff in Jiangxi, China. *J. Earth Sci.* 25, 495–505

Appendix 1.a

Drill core log

A Flintstone Rock - SHEL 82-35

Azimuth: 0 deg.
Dip: 90 deg.

0.0m	-	14.5m	overburden
14.5m	-	91.4m	quartz-breccia
	A5	17.1m	opaque massive quartz, with milky cross-cutting veins, quartz-breccia with kaolin infilling, clast supported
	A4	33.4m	opaque massive quartz, with milky cross veins, hematized fracture stains
	A3	53.0m	massive quartz and veins with vugs (prismatic quartz), multiple phases, kaolinized phenocrysts and infilling
	A2	60.0m	massive quartz, multiple phases, kaolinized phenocrysts, metallic mineralization
	A1	66.2m	angular to subangular milky quartz clasts, breccia clast supported, kaolin infilling
		91.4m	end of hole

Appendix 1.b

Drill core log

B Sabeans Lake - SABL 94-2

Azimuth: 320 deg.
Dip: -50 deg.

0.0	-	4.0 m	overburden
4.0	-	45.3 m	greywacke metasediment
			greenish-grey, fine- to medium- psammite, interbedded 1-5 m zones of finer argillite (pelite), with hornfels and cordierite; variably fractured, silicified zones and quartz veins
45.3	-	102.1 m	quartz breccia
			intense kaolinization (> 5 - 40 %), massive, milky quartz
	B2	80 m	compact kaolin (> 20%), anasmatosing opaque quartz veins
	B1	100 m	kaolinized psammite; cross-cutting quartz, jasper sheet veins and comb-texture milky quartz
102.1	-	182.8 m	greywacke metasediment
		182.8 m	end of hole

Appendix 1.c

Drill core log

C Little Tobeatic Lake - TSZ 94-4

Azimuth: 330 deg.
Dip: -50 deg.

0.0	-	3.5 m	overburden
3.5	-	40.5 m	metasediment: greywacke, silicified quartz veins and fractures
40.5	-	65.0 m	shear zone intense fracturing, limonitic stains; quartz veins; mylonite bands with fine grained pyrite; intense ochre clay alteration, lost core
65.0	-	76.0 m	quartz breccia vuggy to massive, matrix supported; intense kaolin alteration, granitic fragments, stretched K-feldspar grains; shearing cross-cutting polyphase phase quartz veins vugs with crystalline quartz, galena and fine-grained sphalerite pyromorphite crystals in hematized zone (oxidation of galena)
76.0	-	77.8 m	leucomonzogranite
77.8	-	118.0 m	quartz breccia massive, matrix supported, polyphase quartz veins; zones of intense kaolin alteration

	C6	98.2 m	dark red, jasper breccia; fine vein network, cross-cutting silecious; altered chalky feldspar phenocrysts; minor kaolin
	C5	103.6 m	zones of intense kaolin alteration, fragments of leucomonzogranite mylonitic jasper bands, crosscutting
	C4	114 m	zones of intense kaolin alteration; jasper bands, crosscutting
118.0	-	128 m	leucomonzogranite foliated with mylonite bands, altered feldspar zones of kaolin alteration, antastomosing milky quartz veins
128.0	-	131.5 m	quartz breccia varies from matrix to clast supported, fractures polyphase quartz veining
131.5	-	152.5 m	leucomonzogranite
	C3	150.4 m	foliated, sheared fabrics, tension gashes; altered feldspar, chlorite; contact with quartz vein, comb texture
152.5	-	166.0 m	quartz breccia
	C2	161.5 m	jasper cross-cutting veins, polyphase anastomosing quartz veins; zones of intense kaolin alteration; altered chalky feldspar; sheared leucomonzogranite fabric
	C1	165.4 m	jasper breccia, polyphase quartz veins, milky quartz with vugs; siliceous; altered chalky feldspar phenocrysts; minor kaolin veins discordant to shear fabric
166.0	-	174.7 m	leucomonzogranite
		174.7 m	end of hole